PFC/JA-91-36

Compendium of Papers by the Fusion Reactor Studies Group

C. G. Bathke, L. Bromberg, E. A. Chaniotakis,
E. T. Cheng, D. R. Cohn, R. A. Krakowski, R. LeClaire,
F. Najmabadi, J. Schultz, S. Sharafat, P. Titus,
P.-W. Wang, J. E. C. Williams, and the ARIES Team

The 14th IEEE/NPSS Symposium on
Fusion Engineering
San Diego, California
September 30-October 4, 1991

To be published in *IEEE Conference Proceedings*.

Table of Contents

COMMERCIAL REACTORS WITH RESISTIVE MAGNETS

L. Bromberg[†], R.A. Krakowski[‡], E.T. Cheng[*], D.R. Cohn[†], C.G. Bathke[‡] and R. LeClaire[**]

[†] Massachusetts Institute of Technology, Cambridge, MA 02139
[‡] Los Alamos National Laboratory, Los Alamos, NM 87544
[*] TSI Research, Solana Beach, CA 92075
[**] Ballena Systems Company, Los Alamos, MN 87544

Abstract

A cost-based systems model is used to re-examine resistive-coil tokamak power reactors and to examine physics, engineering, and operational tradeoffs needed to project an economically competitive system. The developmental, technological, costs, and operational issues of copper-coil reactors are revisited in light of recent engineering innovations and new developments in physics. The critical isues of engineering innovation (neutronics related) are discussed.

1 Introduction

Interest in normal conducting tokamak reactors is justified because of substantial advantages offered over superconducting magnets.[1,2,3] Some of these advantages include ease of maintenance, minimization of the shield-thickness requirements, and eased developmental path (in the engineering issues) for fusion commercialization.

The technological and operational advantages of using resistive (copper alloy) magnets to generate the toroidal field in a commercial fusion power station must be balanced against the increased costs associated with a more massive fusion power core and the added power needed to supply ohmic dissipation in the magnets. After detailing the technological and operation features and advantages of copper-coil fusion reactors in Section 2 and the neutronic characteristics of the system in Section 3, the tradeoffs are quantitatively evaluated using the cost-based systems model described in Section 4; parametric results are also given in Section 4. A summary and conclusions are given in Section 5. The primary goal of this study is not to generate an optimized design, but rather to identify fertile areas and future directions for improved tokamak power reactors.

2 Engineering Issues

In this section, design issues of resistive tokamak reactors previously addressed are summarized, and innovative engineering features are described. A novel method of increasing the lifetime of the magnet, the self-shielded coil, is analyzed.

Resistive magnets have many advantages over superconducting magnets. The one disadvantage that they have is the resistive power. The power dissipated results in an increased power recirculating fraction for the plant. It can be easily shown[3] that the dissipated power in the toroidal field coil is minimized (at constant weight) by making the cross-section along the coil uniform (i.e., constant current density in the magnet). Under these conditions the dissipated power in a magnet can be estimated by

$$P_{TF} \sim \frac{\rho r_c \sigma}{f}$$

where ρ is the resistivity of the conductor, r_c is the average minor radius of the toroidal field coil, σ are the stresses in the throat, and f is the conductor filling fraction. In order to decrease the recirculated power, the magnet should have low stresses, resulting in large-cross section and low current density. High conductor filling fraction f is also desirable. One consequence of minimizing the dissipated power in the magnet is that problems associated with static or fatigue loads are reduced drastically, an important consideration for pulsed test reactors.

The design approach follows closely the C-MOD tokamak experiment features[4]. The coils are manufactured of simple, jointed sections. Figure 1 shows an elevation view of the toroidal field coil system for a commercial reactor using resistive coils[2]. The main difference between this design and Alcator C-MOD is in the presence of cooling channels in the toroidal field coil, plus the use of a structure through the center of the machine to react the vertical loads. The plates are thick enough to carry the bending created by the vertical Lorenz load, which is reacted by the structure in the inside of the bore and in the outer perimeter of the magnet. The structure through the bore of the machine and the use of thick horizontal plates that can carry most of the in-plane bending minimize the required superstructure on the top and the bottom of the reactor.

The simple sections required, coupled with the low stresses in the toroidal field coil, decreases the unit cost of the toroidal field coil. Thick plates of soft copper (does not require work hardening) can be used. Machining operations can be kept at a minimum, with only polishing and grinding operations required. This results in unit costs for the toroidal field coil that should be comparable to those of the shield. The only exception to the simple machining operation are the cooling channels and the joints. The cooling channels have to be machined (or possibly etched) and then covered. The manifolding can be done inside the plates, minimizing pipe-joining operations (one inlet and outlet per plate). Figure 2 shows a cross-section of a coil section. The tolerance requirements for the joints can be minimized by utilizing spring-loaded contacts, such as used in Alcator C-MOD. Estimates for the unit cost for the toroidal field magnet are \$30-40/kg, which is a factor of 3-4 less than for superconductor magnets, but comparable to the cost of the copper in the superconducting magnets.

Resistive magnets need to be cooled in order to remove the dissipated power and the neutron heating. In order to minimize the power, the temperature of the magnet should be kept low. Due to the low heating power densities, gas cooling of the toroidal field coil can be envisioned. In order to minimize possible interaction between the coolant and the breeding material, helium is a good candidate. Organic coolants could also be considered. Radiolytic decomposition of the gaseous or liquid coolant would not be a major problem for this application, due to the reduced neutron flux at the location of the toroidal field coils. Magnet lifetime limitations due to interaction with radicals produced by radiolysis are therefore eliminated. The reliability of gas cooled, resistive magnets should be high.

Plate magnets also have the advantage of using planar insulation. It is expected that due to the nature of the loading (mostly under compression, with very little shear across the insulation) and the planar nature of the insulation, the choice of materials that can be used for insulation is substantially increased. Inorganic insulations, with much improved neutron irradiation survivability, could be used. Ceramic coatings are regularly manufactured on materials that are of interest for the magnet conductor (aluminum, through the process of anodizing, and on copper). The process is inexpensive.

The shielding required for the magnet can be further minimized by the self-shielded magnet. Since the toroidal field coils are relatively thick and the stresses are small, it is possible to thin the copper conductor in the region close to the plasma,

providing a gap between adjacent coil turns. The insulator can therefore be removed from this region. This results in an increase of the hoop stresses, but since they are small the increase can be tolerated. The lifetime of the magnet is then determined simultaneously by damage of the conductor in the region close to the plasma and the retrieved insulation. The self-shielded magnet is only possible with the use of resistive coils because of the absence of cryogenic load, the allowed increase in the copper resistivity (in superconducting magnets, the copper resistivity determines stability and provides quench protection), and the insensitivity of the conductor and insulation to irradiation. Detailed calculations of the self-shielded magnet are described elsewhere in this conference[5].

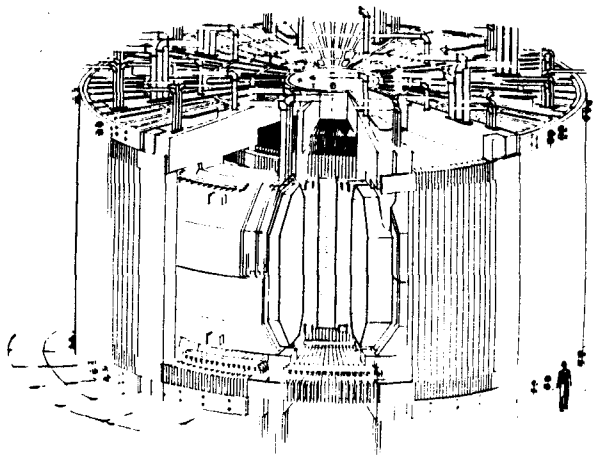

Figure 1. Elevation view of resistive tokamak resistive coil (RC) reactor.

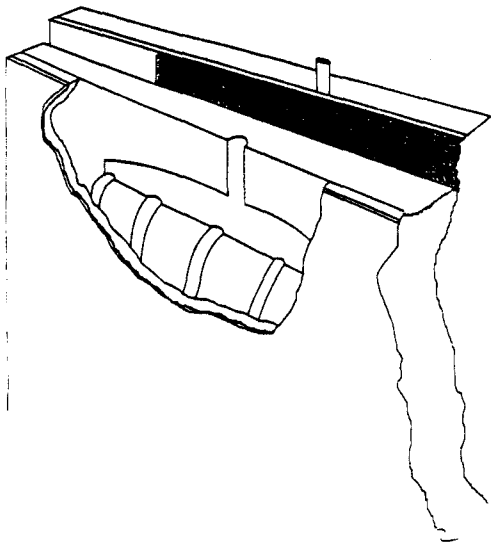

Figure 2. Cross-sectional view of coil element, showing cooling passages.

The poloidal field (PF) could also be normal conducting. With demountable toroidal field coils, the PF system can be placed inside the bore of the toroidal field magnet, as in Alcator C-MOD. The main equilibrium coils, on the plasma outboard, can be placed outside of the magnet and could be made superconducting, in order to decrease by about a factor of 2 the power required for the PF system. Placing the PF system close to the plasma results in significant reduction in the size of the central transformer and the shaping coils.[6,7] The resistive power for the PF system can be decreased by factors of about 2, while the energy in the system can be decreased by factors of 4 as compared with PF systems located exbore of the TF magnet.

The resistive magnet has features that makes it attractive even for short pulse operation. As mentioned above, the stresses in the magnet, in order to minimize the dissipative power of the toroidal field coils, are much smaller than in comparable superconducting designs (in order to keep the dissipated power small). This results in stresses below the endurance limit (fatigue is not an issue). The possibility of placement of the poloidal field coils inside the device also has a large impact on the attractiveness of pulsed operation, minimizing the stored energy. Plasma shaping and control are simplified substantially by the use of internal poloidal field coils.

One of the major advantages of resistive magnets compared with superconducting magnets is the ease of assembly and maintenance. Demountable coils, made possible only by using normal conducting magnets, can be used. Very simple assembly/disassembly operation were described previously[3]. The structure and the toroidal field coil are disassembled after a few steps consisting of simple vertical lifts, providing access to the first wall/vacuum vessel, blanket, and shield. The assembly/disassembly procedures will be tested in Alcator C-MOD. The possibility of early assessing the maintenance characteristics of fusion reactors based on resistive magnets is a clear advantage over those based on non-demountable magnets. Even though Alcator C-MOD maintenance will not be hands-off, the experience gained by taking the device apart and rebuilding it will make clear the operations that require further development. The developmental path of fusion could be substantially simplified if fusion reactors with resistive magnets are cost attractive.

The time required for disassembly of the nuclear island for the periodic change of the first wall and blanket sectors will be substantially reduced compared to superconducting magnets. The effect of decreased downtime (resulting in increased availability) is, however, hard to quantify. In the system study comparison between superconducting and resistive coils shown in the next section, the availability of the reactor was held constant at a nominally high value.

There are about 60 coil sectors, consisting of inboard and outboard vertical legs and horizontal legs. Each coil sector weighs about 150 tonnes, and has a maximum dimension of about 8 m, making it possible to transport sectors manufactured and tested at a factory. The coils could be easily reassembled at the site. If the tritium breeder is liquid, the blanket structure could be raised and lowered as a single unit (if the breeder is bled from the blanket). The same is true of the first wall/vacuum vessel. Rapid assembly would decrease the time required for construction of the power plant, decreasing substantially the interest costs during construction. However, for the work presented in this paper, the construction time has been held fixed for both the superconducting and the resistive magnet cases.

3 Neutronics and Radioactivity

3.A. Calculational Methods and Model

One-dimensional neutronic calculations were done using the coupled neutron and gamma-ray transport code ANISN[8] and ENDF/B-V based nuclear data library, MATXS5[9]. The blanket and magnet are modeled within an infinite cylinder with plasma and scrap-off regions in the center. The radii of plasma and scrap-off regions were assumed to be 1.0 and 1.1 m, respectively.

The blanket neutronics model consists of a 3 mm first wall, a 0.2 m tritium breeding zone, and a 0.4 m reflector. It is followed by a 50 mm coil case and the 0.8 m copper magnet. The first wall and blanket structural material is the V5Ti5Cr alloy. The breeding zone is composed of 10% structure and 90% liquid lithium, all by volume. The reflector is made of 10% structure, 10% liquid lithium, and 80% non-structural vanadium. The coil case is made of ferritic steel and is 95% dense to allow for helium

coolant to pass. The copper magnet is a mixture of 90% copper, 5% insulator, and 5% helium.

Results of calculations varying the Li-6 enrichment in Li were obtained and discussed in the next section.

3.B. Results and Discussion

3.B.1 Tritium Breeding Ratio and Nuclear Heating Rate

Table I shows tritium breeding and nuclear heating rates at the 7.42% (natural), 20%, and 30% Li-6 enrichment factors in lithium. As shown in Table I, the tritium breeding ratios are 1.110, 1.206, and 1.225 tritons per D-T neutron, respectively, when the Li-6 enrichment factors are 7.42, 20, and 30% in lithium. The corresponding blanket energy multiplication factors are 1.18, 1.17, and 1.16, respectively. A sensitivity analysis using a variational technique[10] indicates that the tritium breeding ratio will level off at 1.20 tritons per D-T neutron, when the Li-6 enrichment is between 15 and 20%. Within this Li-6 enrichment factor range, the blanket energy multiplication will be about 1.17. Note that at 20% Li-6 enrichment factor in lithium, the nuclear energy deposited in the coil case and copper magnet is about 3% of that deposited in the blanket. This amount of nuclear energy has to be removed from the magnet together with the ohmic-heating induced energy.

To focus our effort for a more detailed analysis on the resistive magnet, we have thus selected the case with 20% Li-6 in lithium as our reference design. Note that the design with 7.42% Li-6 may result in slightly higher values in all nuclear heating, radiation damage, and activation parameters in the magnet. An example is the nuclear heating rate. As shown in Table I, the total nuclear energy deposited in the magnet is 20% higher (3.4% of the blanket nuclear heating) in the case when the Li-6 enrichment factor is 7.42% in lithium, than when it is 20% in lithium (2.8% of the blanket nuclear heating).

Table I

Tritium Breeding Ratios and Nuclear Heating Rates for the V/Li Fusion Reactors with Resistive Magnets (Li-6 Enrichment Factor in Lithium: 7.42%, 20%, and 30%)

Percent Li-6 in Li	7.42	20	30
Tritium Breeding (T/D-T neutron)			
Li-6(n,α)T	0.777	0.933	0.987
Li-7(n,n'α)T	0.333	0.273	0.238
TBR	1.110	1.206	1.225
Nuclear Heating Rate (MeV/D-T neutron)			
First Wall	0.230	0.219	0.215
Breeding Zone	8.987	9.352	9.522
Reflector	7.460	6.885	6.677
Blanket Total	16.7(1.18)[a]	16.5(1.17)	16.4(1.16)
Coil Case	0.171	0.123	0.105
Copper Magnet	0.396	0.330	0.300
Magnet Total	0.57(3.4%)[b]	0.45(2.8%)	0.41(2.5%)

[a] Blanket energy multiplication factor.
[b] Relative to total energy deposited in the blanket.

3.B.2. Radiation Damage to the Resistive Copper Magnet

For the operation of a resistive copper magnet, the most sensitive parameters due to neutron and gamma-ray irradiation are probably the nuclear heat dose to the insulator and production of other elements due to neutron transmutation. The spacial distribution of radiation dose rate (per full power year at 1 MW/m^2) to the insulator in the copper magnet is given in Table II. The corresponding volumetric coil nuclear heating rates and fast neutron fluxes are also displayed in Table II for comparison. As shown in Table II, the radiation dose rate to the insulator is 1.51×10^9 Gy per MW-y/m^2 at the location immediately behind the coil case. At the location 0.4 m from the coil case, the radiation dose rate drops to 1.36×10^7 Gy per MW-y/m^2, about two orders of magnitude lower. At this location the overall radiation dose to the insulator will be 2.04×10^9 Gy when the total first wall exposure is 150 MW-y/m^2 which is more than the expected lifetime exposure (30 full power years at 5 MW/m^2 wall loading). If polyamide-based insulator (Spaulrad-S) is employed for the resistive magnet, the location mentioned above should be ideal to begin installation of insulator materials in the self-shielded coils, since the postulated lifetime radiation dose for such insulators[11] is 4.0×10^9 Gy.

Table II

Radiation Dose Rates, Fast Neutron Fluxes and Volumetric Nuclear Heating Rates in the Copper Magnet of the Reference Commercial Fusion Reactor at 1 MW/m^2 Neutron Wall Load (20% Li-6 in Lithium)

Distance From Coil Case (cm)	Insulation Radiation Dose Rate (Gy/y)	Fast Neutron Flux (n/m^2/y)	Coil Volumetric Nuclear Heating Rate (W/cm^3)
0.5	1.35×10^9	1.43×10^{20}	1.46×10^{-1}
9.5	4.97×10^8	5.46×10^{19}	5.91×10^{-2}
19.5	1.52×10^8	1.75×10^{19}	1.81×10^{-2}
29.5	4.55×10^7	5.32×10^{18}	5.59×10^{-3}
39.5	1.33×10^7	1.55×10^{18}	1.71×10^{-3}
49.5	3.82×10^6	4.38×10^{17}	5.10×10^{-3}

3.B.3. Afterheat

The neutron activation calculations were performed with the activation calculation code REAC and associated decay data and activation cross-section libraries[12]. In these calculations we assumed a neutron wall loading of 5 MW/m^2. There were 8 cycles of operations during the lifetime of the copper magnet. Each cycle has a continuous, full power operation of 4 years, and a subsequent shutdown for one year for maintenance. At the end of lifetime, i.e., the end of the 8th cycle, the total neutron fluence at the first wall region is 160 MW-y/m^2.

Table III shows the afterheat heating values at the copper magnet after the 1st and 8th (last) cycle of operation. These afterheat heating values, both power densities and accumulated energies, should be taken into account for normal operation and abnormal safety considerations. In Table III, both maximum (represented at the location 0.5 cm from the coil case) and averaged (over the 0.4 m magnet region closest to the coil case) values are given at one minute, one hour, and one day after shutdown. The maximum and averaged afterheat heating values, as shown in Table III, are 4.7 and 3.3% of the operating power density, respectively, at one minute after shutdown. They drop to 1.5% and 0.97%, respectively, at one hour after shutdown. At one day after shutdown, the afterheat power densities drop further to 0.48 and 0.32%, respectively.

Table III

Maximum (0.5 cm from Coil Case) and Averaged Afterheat Power Densities in the Copper Magnet at the End of First and Last Cycles (5 MW/m^2 Neutron Wall Loading)

Time After Shutdown	1 min.		1 hour		1 day	
Maximum	W/cm^3	%[a]	W/cm^3	%	W/cm^3	%
End of First Cycle	0.0349	4.7	0.0106	1.4	0.00324	0.43
End of Last Cycle	0.0352	4.7	0.0110	1.5	0.00359	0.48
Averaged Values (End of Last Cycle)	0.00572	3.3	0.00169	0.97	0.000553	0.32

[a] Percent of operating power density.

3.B.4. Transmutation

Table IV shows the concentrations of elements due to neutron transmutation in the copper magnet. These elements and their concentrations in copper should be considered in the design of the resistive copper magnet for the operation of the commercial fusion reactor. As shown in Table IV, nickel appears to be the element showing the maximum concentration among all other elements due to transmutation. It is followed by zinc. At the end of the last cycle (lifetime irradiation, 160 MW-y/m^2), the maximum concentrations of nickel and zinc in the magnet are about 7600 and 1700 ppm, respectively. The averaged concentrations are, however, about 1200 and 280 ppm, respectively. The other significant elements due to transmutation are cobalt, hydrogen, and helium. The lifetime maximum concentrations for Co, H, and He, are about 6, 70, and 20 ppm, respectively, while the averaged concentrations are 1, 10, and 3 ppm, respectively.

Table IV

Maximum and Averaged Concentrations (ppm) of Elements Due to Neutron Transmutation in the Copper Magnet at the End of First and Last Cycles (5 MW/m^2 Neutron Wall Loading)

Element	0.5 cm from Coil Case First Cycle	0.5 cm from Coil Case Last Cycle	Averaged Last Cycle
Cobalt	2.5	5.9	0.89
Nickel	943	7567	1174
Hydrogen	8.3	65	9.6
Zinc	214	1681	281
Helium	2.4	20	3.1

3.B.5. Recycling and Waste Disposal of Copper Magnet

After the lifetime operation, the copper magnet can be either disposed of as low-level nuclear waste or recycled after cooling. Recycling of copper magnet appears to be a more attractive option for fusion energy development. The contact dose rates for handling the copper melt were estimated for the main copper material and potential impurity elements. The results are displayed in Table V. Cobalt-60 is the main radionuclide produced in copper to contribute a significant level of gamma-ray dose rate. However, as shown in Table V the contact dose rate due to Co60 will decay to 1.5 mR/h, which is below the hands-on level, after 100 years cooling time.

At 100 years cooling time, the impurity elements may still impose non-negligible contact dose rates. As shown in Table V, the contact dose rates due to 1 ppm of impurity elements Ag, Nb, Tb, Ho, and Eu, are 48, 4.6, 0.4, 11, and 13 mR/h, respectively. To lower the contact dose rate below 1 mR/h, the impurity levels for Ag, Nb, Ho, and Eu should be controlled below 21 ppb, 0.22 ppm, 91 ppb, and 77 ppb, respectively.

As far as the issue of waste disposal is concerned, the copper material itself will meet the criteria for 10 CFR 61 Class C waste disposal[13]. The only important long-lived radionuclide produced in copper is Ni63 (half-life 100 y). The Class C waste disposal rating due to Ni63 at the end of lifetime operation is 0.002. The waste disposal ratings due to 1 ppm of impurity elements Ag, Nb, Ho, if present in copper, are 0.13, 0.05, and 0.24, respectively. The waste disposal ratings due to Tb and Eu, however, are negligibly small compared to that for Ag, Nb, and Ho.

Table V

Contact Biological Dose Rates Due to Copper and Several Important Impurity Elements (After 160 MW-y/m^2 Lifetime Irradiation)

Element	Dominating Radionuclide	Half-life (y)	Contact Dose Rate (mR/h)
Copper (Main)	Co60	5.27	1.5 [†]
Silver[‡]	Ag108m	127	48
Niobium	Nb94	20000	4.6
Terbium	Tb158	150	0.4
Homium	Ho166m	1200	11
Europium	Eu152	13.3	13[†]

[†] 100 y cooling.

[‡] Impurity levels for these elements (Ag, Nb, Tb, Ho and Eu) are assumed to be 1 ppm.

4 Systems Analysis

4.A. Model

A detailed description of the parametric physics and engineering systems model utilized in this study is given in reference 14, with a brief summary and application to the study of pulsed tokamak reactors being described in reference 15. Specifying the net-electric power, P_E, for a given fusion-power-core (FPC) configuration (i.e., minor radius a, plasma aspect ratio A, a range of plasma standoff distances, recirculating power requirements, etc.) determines the required fusion power and the magnetic field for a given equilibrium/stability scaling (i.e., plasma safety factor q, and beta scaling). Generally q is fixed and a Troyon-like scaling is used (i.e., $\beta = C_T I_\phi / B_\phi a$, where C_T is nominally a constant, I_ϕ is the plasma current, and B_ϕ is the TF field at the plasma); the constant $C_T = \epsilon\beta_p/(5q^*)$, where $\epsilon = 1/A$, β_p is the plasma pressure normalized to the pressure of the poloidal magnetic field, and $q^* = q(1-\epsilon)^2$ is fixed by choices of $\epsilon\beta_p$ and q^* that are appropriate to first or second-stability region tokamak plasmas [16]. For a specified average plasma temperature, pressure balance and nominal assumptions about hot-ion pressure and impurity levels determine the plasma densities; a simplified plasma energy balance gives the global confinement time required to meet the above-stated conditions (i.e., the confinement time is a constraining result and not a constraining input). The level of tokamak plasma modeling is generally that described by Uckan [17].

The dissipated power in the magnets, along with the fast-wave current-drive power, represents the main components of the recirculating power, with the cost of the latter representing an important tradeoff with the capital cost of the FPC. The FPC mass and the power recirculated to sustain the plasma are used to estimate the related capital costs, which are expressed as annual charge that includes modern levels of contingency and indirect costs [18]. Once normalized to the annual net-energy output, the resulting incremental cost of electricity, ΔCOE, reflects the added cost of generating power from the magnetic fusion system that is more capital-intensive than fission. The

ΔCOE includes the incremental primary-heat-transport (PHT) and balance-of-plant (BOP) items needed to deliver recirculating power to the FPC; ΔCOE is the main object function used in the systems model. The economically acceptable magnitude of ΔCOE is determined largely by cost credits related to fuel supply and safety/environmental advantages.

Table VI lists a set of parameters used to establish a "point-of-departure" case about which parametric variations and design sensitivity studies are conducted. Using this nominal point-of-departure case, a standard parameter search varies the plasma geometry (a and A) for a fixed net-electric power and reports a minimum ΔCOE value; the sensitivity of the minimum incremental cost to changes in key parameters listed in Table VI is then used to identify optimal operating regimes for the resistive-coil tokamak reactor.

4.B. Results

The systems model scans a broadly specified range of minor radius and aspect ratio for the nominally fixed, point-of-departure conditions summarized in Table VI. The dependence of key cost and reactor parameters on the minor radius a for $A = 3$ is shown on Figure 3, with Figure 4 summarizing the dependence of ΔCOE on a and A. The absolute minimum-ΔCOE point corresponds to $A = 2.6$, $a = 1.9$ m, ΔCOE = 31 mill/kWehr for the resistive magnet reactor, while the corresponding superconductor-coil (SC) case gives ΔCOE = 13 mill/kWehr at $A = 2.5$ and $a = 1.6$ m. Low aspect ratio, intermediate size machines minimize the COE.

The breadth of the operating space available to the RC option is conveniently illustrated in a space defined by plasma current, peak TF coil field, and geometry. Figure 5 shows this reactor operating space along with contours of constant ΔCOE. Generally, the large costs associated with compensating for resistive magnet losses and with the relatively massive TF coils drive the resistive coil reactor to relatively small aspect ratio and maximum beta values. Because of the SSR plasma scaling assumed ($C_T = 0.15$ T m/MA for $q^* = 4.0$ and $\epsilon\beta_p = 3$, giving $\beta = 0.15$), the current ($I_\phi = 8.3$ MA) and current-drive requirement (bootstrap fraction = 0.7) are small, giving an even stronger impetus to minimize FPC mass while maximizing the TF coil cross-section available to transport current.

The TF coil current density selected for the point of departure case ($j_{TFC} = 6$ MA/m^2) is based on the results of a detailed optimization study. The outer 75% of the TF coil cross-section is increased in area by the factor $1/f_{XS}$, further minimizing the ΔCOE.

The ratio of contributions to ΔCOE for the resistive coil case from FPC/current drive/TF coil losses is 0.43/0.15/0.42. The impact of reducing the assumed mass ratio of PF coil to TF coil ($f_{PFC} = 0.50$) and the composite unit cost of the FPC ($c_{FPC} = 50$ \$/kg) on ΔCOE is shown on Figure 6, which also includes the effect of beta (i.e., CT through variation of $\epsilon\beta_p$ for $q^* = 4$). Since the already optimized coil mass has only a 43% leverage on ΔCOE, reduction in f_{PFC} has a relatively small effect. A change with greater impact would be a reduction in the unit cost of the magnet set, with the sensitivity shown on Figure 6 corresponding to the more realistic value of $f_{PFC} = 0.1$ (i.e., taking into account the larger weight of the toroidal field coil and the decrease weight of the poloidal field coil due to the use of internal coils). For the more realistic case of \$30/kg for the coil and $f_{PFC} = 0.1$, then ΔCOE $\sim$ 24 mill/kWehr, still about 10 mills kWehr more expensive than the comparable SSR.

The decrease in ΔCOE with increased beta (i.e., increased $\epsilon\beta_p$) depicted in Figure 6 is examined further in Figure 7. Increased $\epsilon\beta_p$ leads to substantial increases in both MPD and Q_E, giving rise to significant decreases in ΔCOE.

Substantial decreases in ΔCOE are predicted for modest increases in the plant capacity, P_E, as is illustrated in Figure 8. These cost decreases again result from increases in both Q_E and MPD for these optimized RC tokamak power plants. Generally, higher plant capacity leads to lower costs for the following reasons: a) economies of scale are built into the unit cost scaling relationships; and b) for the SSR/RC cases the recirculating power losses scale primarily as B_ϕ^2, whereas the power output scales as B_ϕ^4; together with the strong economic incentive to minimize the mass of an already sizable FPC, a stronger-than-usual economy of scale results (ΔCOE$\sim P_E^{-0.8}$).

Table VI
Typical Physics, Engineering, and Costing Parameters[a]

Physics Parameters	
$\epsilon\beta_p$	3.0
q^*	4.0
Elongation	1.8
Average temperature (keV)	20.
Plasma profile factors	
density	1.0
temperature	1.0
Current-drive efficiency (10^{20}A/m^{2}W)	0.3
Bootstrap fraction	0.7
Standoffs (m)	
inboard	0.60(1.30)
outboard	0.60(1.50)
top/bottom-side	0.60(1.50)
plasma scrapeoff	0.10
Blanket energy multiplication	1.20
Thermal conversion efficiency	0.40
Net-electric power	1000
Current-drive efficiency	0.60
Plant capacity factor	0.75
PF coil/TF coil mass ratio	0.50
TF coil properties	
conductor	Cu
current density (MA/m^2)	6.
filling fraction	0.80
resistivity (Ω/m)	2.0 10^{-8}
Costing parameters	
Unit costs	
FPC(\$/kg)	50.(100.)
Current-drive power supplies(\$/W)	2.0
Thermal power handling, (\$/W)	$400/P_{TH}^{0.45}$
Electrical power handling/conversion[19]	
turbine plant equipment	$7.0/P_{ET}^{0.17}$
electric plant equipment	$4262/P_E T^{0.51}$
miscellaneous plant equipment	$252/P_{ET}^{0.41}$
Indirect cost factor	0.9
Fixed charge rate (1/yr)	0.1

[a] values in parentheses are used to model the SC comparison case.

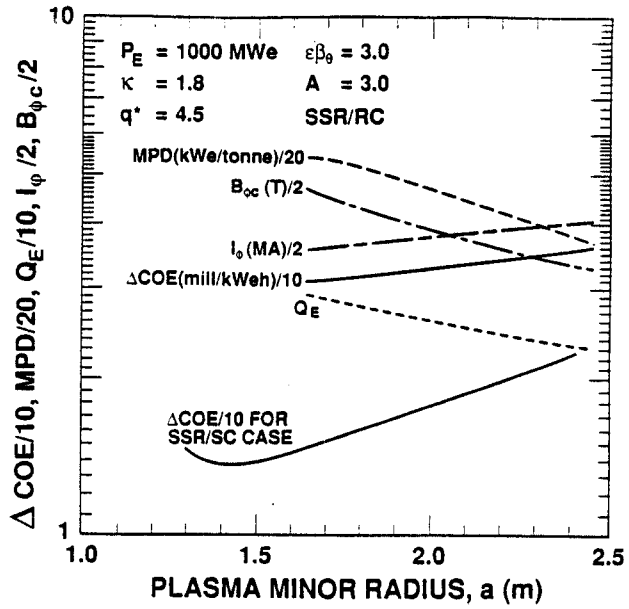

Figure 3. Dependence of key economic and reactor parameters on plasma minor radius for $A = 3$.

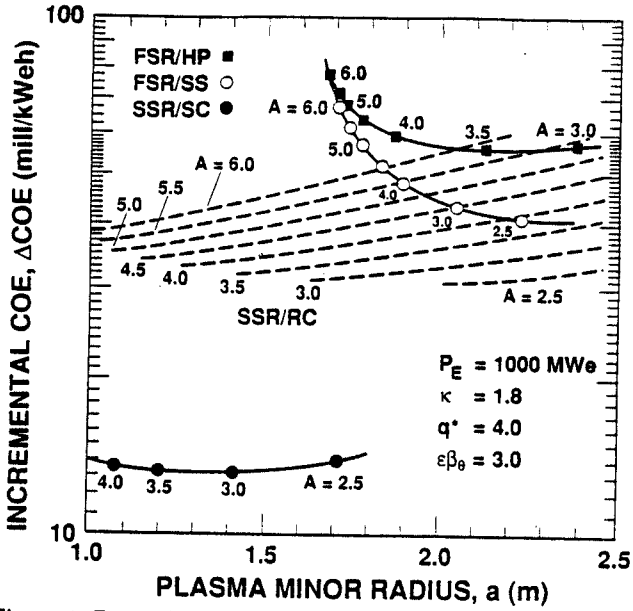

Figure 4. Dependence of incremental cost of electricity on plasma configuration.

5 Summary and Conclusions

The following conclusions have been reached:

- β values of at least 0.10 are needed, and ideally would like to have values 0.15 (Figure 7).
- Second stability is needed not only for the high beta, but also to hold the current-drive power to low levels.
- Optimum TF coil current densities are near 6 MA/m^2 for the unit costs used, and optimization of TF coil cross-section has a small impact on cost.
- RC tokamak reactors have a strong economy of scale (Figure 8).
- Given that the non-fusion balance of plant adds 25 mill/kWehr, the 1000-MWe(net) RC tokamak power plant will cost 15% more than a SC version using the same advanced physics, assuming comparable capacity factor and construction times.

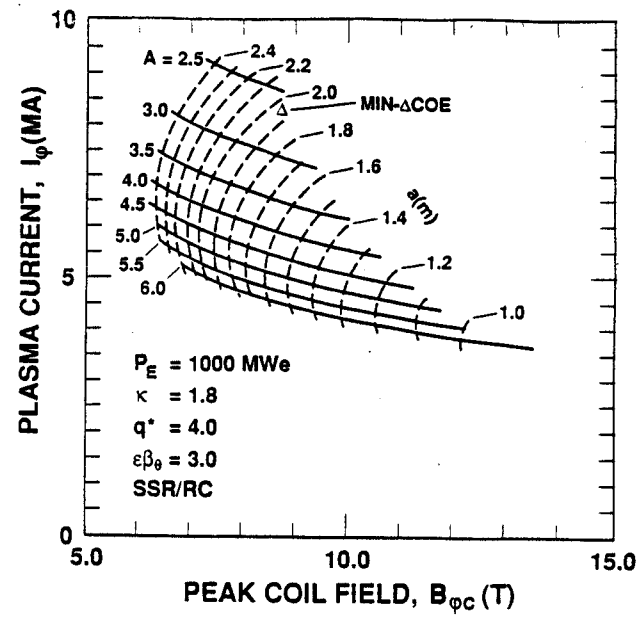

Figure 5. Operating space for a resistive-coil tokamak reactor showing contours of constant minor radius and constant incremental cost of electricity.

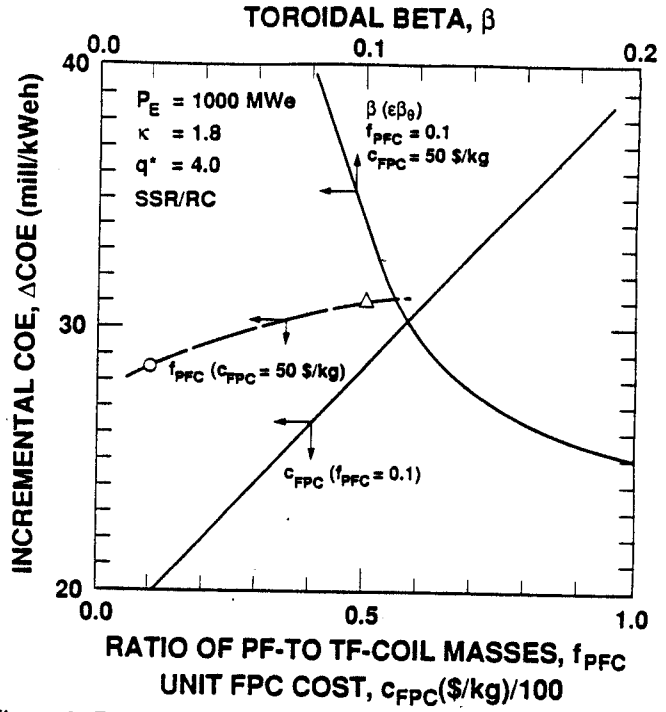

Figure 6. Dependence of incremental cost of electricity on relative PF coil mass, unit cost of FPC, and toroidal β ($\epsilon\beta_p$).

Simplification of the nuclear island, together with increased reliability and ease of maintenance, would decrease the required developmental path for fusion commercialization. Furthermore, decreases in construction time could minimize the cost increment due to the large size of nuclear island and the increased recirculating fraction. If high plant factors and decreased R&D and construction time prove realistic for the resistive tokamak reactors, then the resistive and superconducting reactors, operating in second stability, would be of comparable costs.

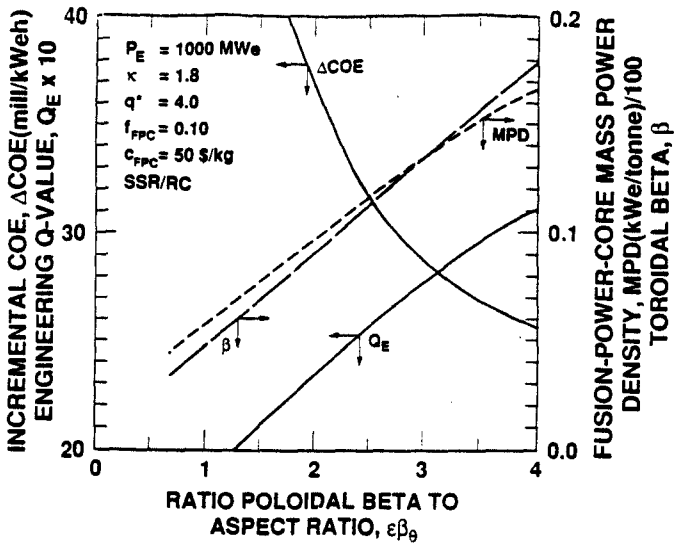

Figure 7. Dependence of incremental cost of electricity on $\epsilon\beta_p$.

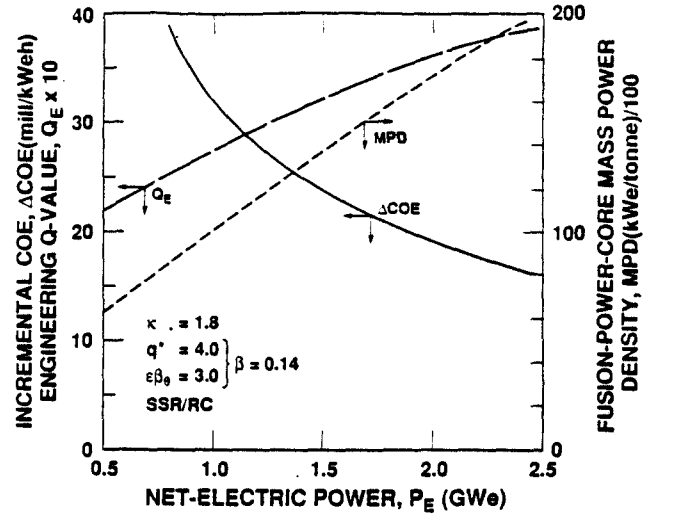

Figure 8. Dependence of incremental cost of electricity on plant capacity.

This work was supported by the U. S. Department of Energy Contract No. DE-FG02-91ER-54110.

References

[1] D.L. Jassby, Princeton Plasma Physics Laboratory Report PPPL-1700 (1980).

[2] L. Bromberg, D.R. Cohn and D.L. Jassby, Fusion Tech. **6** 597 (1984).

[3] R.J. Leclaire, R.E. Potok, L. Bromberg, et al., Fusion Tech. **8** 327 (1985).

[4] See, for example, S. Fairfax, this conference.

[5] L. Bromberg, D.R. Cohn, E.A. Chaniotakis and P.W. Wang, "Long Pulse Tokamaks using High Performance Resistive Magnets," presented in these proceedings.

[6] D.L. Jassby, R.A. Jacobsen, J. Kalnavarns, L.S. Masson and J.P. Sekot, "Resistive Demountable Toroidal Field Coils for Tokamak Reactors," Princeton Plasma Physics Laboratory Report 1809 (July 1981).

[7] T.F. Yang, R.J. LeClaire, E. Bobrov, L. Bromberg, D.R. Cohn and J.E.C. Williams, "A Demountable Copper TF Coil System for Ignition Test Experiments and Commercial Reactors," Fusion Tech. **8** 838 (1985).

[8] W.W. Engle, Jr., "A User's Manual for ANISN," K-1693, Oak Ridge Gaseous Diffusion Plant (1967).

[9] R.E. MacFarlane, "TRANSX-CTR: A Code for Interfacing MATXS Cross Section Libraries to Nuclear Transport Codes for Fusion System Analysis," Los Alamos National Laboratory Report, LA-9863-MS (1984).

[10] E.T. Cheng and R.W. Conn, "The Influence of Design Variations on Controlled Thermonuclear Reactor Blanket Neutronic Performance Using Variational Techniques," Nucl. Sci. Eng. **62** 601 (1977).

[11] R. Schmunk, et al., "Test on Irradiated Magnet Insulator Materials," J. Nucl. Mat., **122 and 123** 1381 (1984).

[12] F.M. Mann, "REAC2: Status of Codes and Libraries," Fusion Tech., **15** 449 (1989).

[13] S. Fetter, et al., "Long-Term Radioactive Waste from Fusion Reactors: Part II," Fusion. Eng. Design, **13** 239 (1990).

[14] R. A. Krakowski and R. L. Miller, "In Search of an Economical Tokamak Reactor," Los Alamos National Laboratory Report (in preparation, 1991).

[15] R. A. Krakowski, R. L. Miller, and C. G. Bathke, "A Cost-Based Systems Analysis of Long-Pulsed versus Steady-State Tokamak Reactors," these proceedings.

[16] G. A. Navratil and T. C. Marshall, "High-Beta Tokamak Operation in the Second Stability Regime," Comm. Plas. Phys. Contr. Fus., **10(4)** 185 (1984).

[17] N. A. Uckan, "ITER Physics Guidelines" International Thermonuclear Experimental Reactor report ITER-TN-8-6 (Nov 1988)

[18] C.G. Bathke, K. A. Werley, R.L. Miller, and R.A. Krakowski, "The ARIES-III D-^{3}He Tokamak Reactor: Design-Point Determination and Parametric Study," these proceedings.

[19] R. L. Miller, W. R. Spears, R. Hancox, and R. A. Krakowski, "Comparison of EURATOM and US Estimates of Fusion Reactor Costs," Fus. Tech., **19(3)** 813 (1991).

LONG PULSE TOKAMAKS USING HIGH PERFORMANCE RESISTIVE MAGNETS

L. Bromberg, D.R. Cohn, E. A. Chaniotakis, and P.-W.Wang
Plasma Fusion Center
Massachusetts Institute of Technology
Cambridge, Ma 02139

Abstract

Engineering aspects of tokamak designs which could address the physics of long pulse hydrogen/deuterium operation and alpha particle dominated heating (Q >5) are presented. The main characteristics of these designs are their relatively small size, their resistive toroidal field coils, and their long pulse capability. In D-T operation this machine could satisfy the basic physics requirements for the ITER physics mission at a much lower cost than the present superconducting ITER design. For these designs demountable TF coils similar to Alcator C-MOD are considered, and steady state water cooling of the magnets is investigated. The demountable nature of the toroidal field magnet simplifies the assembly and maintenance operations. Internal poloidal field coils minimize this system and increase its flexibility.

1. Introduction

Interest in normal conducting tokamak experiments is justified because of substantial advantages offered over superconducting magnets[1,2,3]. Some of these advantages include: ease of maintenance, internal poloidal field coil, minimization of the shield-thickness requirements, and construction costs. The main disadvantage, the required power for the toroidal field coil, is not a large factor for experimental reactors. The cost of the required electricity is an operational cost, not a capital cost. Although the power supplies to drive the system are larger than for superconducting magnet designs, many laboratories have the required equipment.

The use of demountable coils has been a common approach for design and construction of tokamak experiments. The flexibility of the devices, in part due to the ease of assembly and disassembly, has facilitated the upgrade of several of the tokamaks with demountable coils[4].

The added flexibility that can be obtained by using the Alcator C-MOD configuration[5] greatly enhances the experimental capabilities. The use of sliding joints eases the process of putting the sectors together by removing the complex assembly step of the different sections, as in Big-Dee. Alcator C-MOD was assembled, from previously unassembled pieces, in about two months. It is estimated that disassembly/reassembly operation will be reduced even further after some experience is gained. Such a construction would be ideal for experimental machines where changing the first-wall, the divertor assembly, etc., is frequent. It also allows for reduced construction time.

The Alcator C-MOD has recently started operation and is presently undergoing testing. The purpose of this paper is to determine the implications of this type of magnet construction to future experiments. Two types of experiments will be described: long pulse, compact, hydrogen experiment, and a long pulse, D-T high Q experiment. The hydrogen experiment would have pulse lengths of about 60 s, inductively induced to decrease dependence on non-inductive current drive. The long pulse ignition experiment would have longer inductive pulse lengths, and it could run quasi-steady state using non-inductive current drive. An accompanying paper describes the requirements for commercial tokamak reactors with resistive magnets[6].

Some of the engineering features of the hydrogen and the long pulse high-Q reactor will be described in this paper. In Section 2 the design parameters are presented. Section 3 concentrates on the toroidal field coil, the configuration and the cooling. Section 4 concentrates on the poloidal field system for these devices. Section 5 describes novel ideas for the vacuum vessel. Finally, Section 6 summarizes the results and identifies areas for additional work.

2. Basic Parameters

Various design configurations are investigated. In particular, the small R = 1.95 m machine whose parameters are given in Table I can be used to study issues associated with long pulse operation in hydrogen or plasmas. In addition the water-cooled R= 3.5 m machine whose parameters are given in Table II is suitable for D-T operation and is capable of addressing the basic physics mission at a much lower cost than the present ITER design[7].

3. Toroidal Field Magnet

There are several advantages of scaling up the size of the Alcator C-MOD toroidal field coil. They have to do with the location of the joint, the support for the poloidal field coil, the design of the sliding joints, and the cooling of the magnet.

Figure 1 shows the proposed modification of the inner leg of the toroidal field coil for both of the designs. The long pulse operation of the magnet minimizes the problem of current penetration into the magnet plates. In Alcator C-MOD, a short pulse machine, the toroidal field current stays near the bore of the magnet, increasing the current density there, making the design of the joint difficult. Additionally, there was insufficient space to make the joint in the inner leg due to the small thickness of the plates. These problems forced Alcator C-MOD to locate the joint in the horizontal leg, rather than in the inner leg[5]. By operating long pulse, the rate of charge-up and shutdown of the toroidal field coil can be reduced to minimize the problems associated with penetration of the current. Also, scaling-up the size of the machine increases the area in the inner leg necessary to make the joint between the horizontal and inner sectors of the magnet.

Locating the joint in the inner leg removes most of the vertical forces from the inner leg. This minimizes the stresses in the inner leg, allowing the use of unreinforced copper and results in both easier design and less expensive magnets. In Alcator-C-MOD the inner leg carries a substantial fraction of the vertical load since the joint is in the horizontal leg which results in a substantial radial component of the TF and current density around the bend.

Table I

Illustrative Long Pulse Machine Parameters
Hydrogen and Long Pulse Design

	Hydrogen	
	High Performance	Long Pulse
Major radius (m)	1.95	
Minor radius (m)	0.65	
Toroidal field (T)	9	6.2
Plasma current (MA)	8.9	6.1
Volt-sec. burn	3	9.2
Pulse length (s)	10	60
Peak OH stress (MPa)	140	110
OH temp. est. (K)	100	280
OH thickness (m)	0.13	0.13
TF stress (MPa)	210	100
TF temp., est. (K)	135	180
TF Power, 77 K	64(77 K)	30(77 K)
Current density (kA/cm^2)	3.2	2.
Stored energy (GJ)	2.7	1.3
Weight (tonnes)	420	420

Table II

Illustrative Long Pulse Machine Parameters
High-Q Design

	DT Operation Water Cooled
Major radius (m)	3.5
Minor radius (m)	1.1
Toroidal field (T)	7.7
Plasma current (MA)	14.2
Volt-sec. burn	90
Pulse length (s)	SS
Peak OH stress (MPa)	100
OH temp. est (K)	SS
OH thickness (m)	0.30
TF stress (MPa)	200
TF temp., est. (K)	RT
TF Power, 77 K	550
Current density (kA/cm^2)	1.6
Stored energy (GJ)	10.3
Weight (tonnes)	2050

Increasing the size of the machine also decreases the current density, even for comparable fields. This is due to the fact that the current scales linearly with size, while the cross-sectional area scales as the square of the size. The current density across the joints is also decreased, making the sliding joint design less demanding than in Alcator C-MOD. By increasing the number of steps, it is possible to decrease the heating in the area of the joint. This is shown schematically in Figure 2.

Another advantage of increasing the size and decreasing the current density and the stresses of the toroidal field coil is the opening of the throat of the magnet. This allows the location of a bolting post along the main axis of the tokamak. In comparison to IGNITOR, where the central post carries both vertical and radial loads, this design's bolting post carries only vertical stresses (the radial stresses are supported by the magnet through wedging).

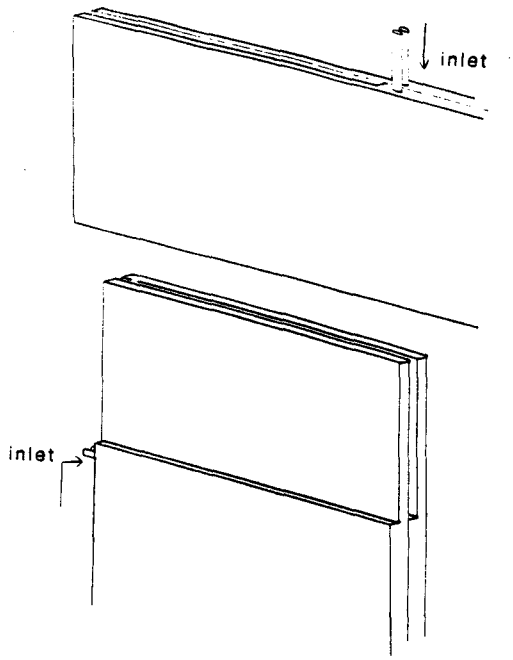

Figure 1. Schematic diagram of inner leg joint. Possible location of cooling connections are indicated.

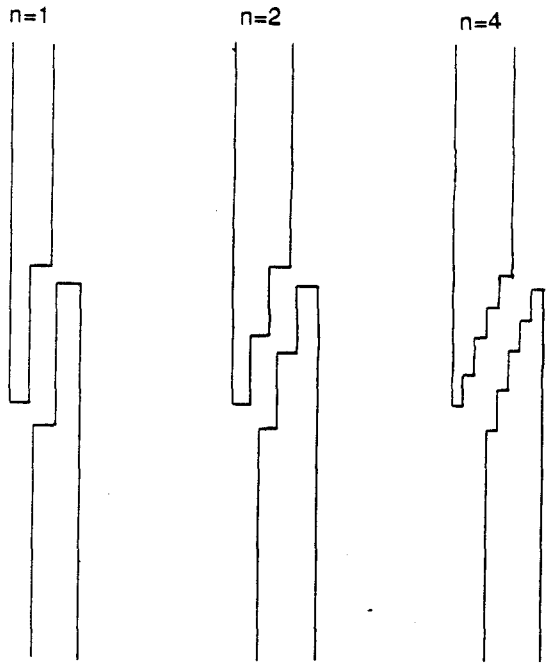

Figure 2. Multiple-step joint and associated current and heat peaking.

It is possible to react most of the loads that would have been carried by the throat of the magnet through this cross-section if a strong bolting post material is used. The net result of carrying these loads through the center of the magnet rather than through the outside is that the size of the superstructure is minimized. The design of the bolting post and its connection to the horizontal legs is one of the outstanding issues that needs future work.

The toroidal field coils would be cooled by water or liquid nitrogen cooling through channels imbedded in the magnet, as shown in Figure 3. After manufacturing the coolant channels and the manifolds, a second thinner copper sheet is soldered via a low temperature process, enclosing the channels. This design prevents direct contact between the coolant and the insulation, extending the lifetime of the magnets. The channels are manufactured in one side of the plates, together with manifolding. This reduces the number of coolant connections to the plates to one inlet and one outlet per plate section.

The joint is in the opposite side of the plates where the cooling channels are located, as shown in Figure 3. The area of the joint is cooled in this manner. To minimize the increase in stress due to the presence of the cooling channels, the cooling channels are not round but elongated in the direction perpendicular to the face of the plates, as shown in Figure 3.

Table III shows typical parameters for the cooling of the toroidal field magnet. The numbers have been calculated for the inner leg of the toroidal field coil, but they are also applicable to the outer section. Typically, the horizontal legs are about half as long as the inner and outer legs are tall. The resistive power shown in Table III refers to the total magnet power requirement.

The self-shielded magnet concept could be utilized for the case of ignited operation[8]. The concept is shown in Figure 4. Basically, the insulation is recessed in the area next to the plasma. The copper plates are thinned in this area, using air as an insulator. The uninsulated section of the plates serves as a shield to the insulation that is located deep in the magnet. Since the lifetime of the copper is orders of magnitude greater than that of the insulation, the magnet lifetime would still be determined by survival of the protected insulation. The shielding required is therefore minimized. Calculations indicate that the copper in the self-shielded magnet decreases the damage to the insulation by an order of magnitude for every 20 cm of magnet that is not insulated[8]. Problems with waste disposal of the magnet are not serious if the magnet is allowed to cool for 100 years[8].

Alcator C-MOD type magnets could be insulated with ceramic material sprayed on its sides. Since the lifetime of ceramic insulation under compressive loads is one to two orders of magnitude longer than for comparable organic insulation, long lifetime of the magnet under neutron damage could be obtained.

4. Poloidal Field Coils

The use of internal field coils minimizes the system required to induce the plasma current and shape the plasma. Long pulse lengths, about 100 s for the small machine and as long as 500 s for the larger machine, have been studied. The power, energy, and stresses of the system are substantially smaller than in the case of the external poloidal field coils. Having the coils relatively close to the plasma also helps with the control of the vertical instability, a consequence of highly elongated plasmas.

Scaling-up the Alcator C-MOD configuration has substantial advantages for the poloidal field system. The lip required for locating the joint in the horizontal leg prevented the central transformer from being inserted with the vacuum vessel, and the central transformer had to be integrated with the inner leg, instead of the vacuum vessel. By removing the lip required in the inner leg it is possible to remove the central transformer, making repairs on the central solenoid easier. The inner leg of the toroidal field can also be maintained, since the central solenoid is not wound on it.

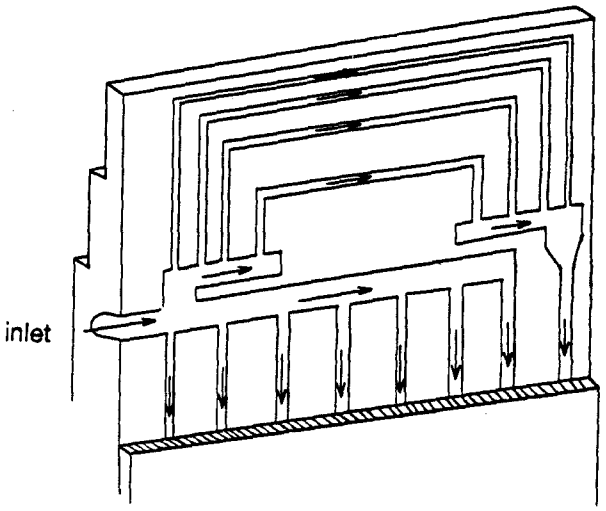

Figure 3. Joint and plate cooling configuration.

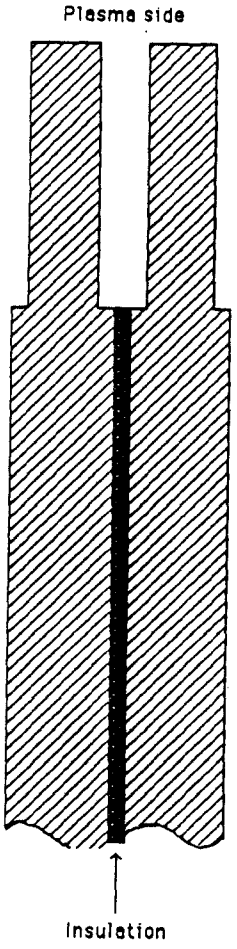

Figure 4. Self-shielded magnet concept.

Poloidal field equilibria for low β and end-of-flat-top for the small, hydrogen machine are shown in Figures 5a and 5b, respectively. The PF shown in Figures 5a and 5b provides 10 Vs for the flat-top. Depending on the electron temperature, the pulse length may be as long as 100 s. Figures 6a, 6b, and 6c show the energy, power, and temperature for a 60 s scenario.

In Table IV the parameters for the PF system of the long pulse 1.95 m machine are summarized.

For the case of the ignited plasma, the poloidal field will undergo a radiation damage rate larger than the toroidal field coil. To handle the larger doses, a radiation resistant conductor is proposed, shown in Figure 7. The conductor has an internal cooling channel and is insulated by radiation-resistant ceramic powder insulator, such as SPINEL. The insulation is held in place by an external sheath. The radiation-resistant insulator decreases the conductor fraction, but with the internal poloidal field coils, the amount of required conductor is minimized substantially.

Table III

Parameters for Forced Flow Coolant
Liquid Nitrogen Versus Water Cooling

	LN_2	Water
Cooling requirements (MW)	55	320
Evaporation of liquid nitrogen (kg/s)	300	NA
Total evaporation, 100 s pulse (tonnes)	30	NA
Bath temp. (K)	77	NA
Bath pressure (MPa)	0.1	NA
Coolant properties of inner leg:		
Total mass flow through magnet (kg/s)	840	840
Mass flux/coil (kg/m^2-s)	5625	5625
Inlet pressure (MPa)	1.6	1.6
Inlet temp. (K)	78.0	310
Coolant current area (cm^2)	6.8	6.8
Flow area (cm^2)	0.8	0.8
Magnet current density (kA/cm^2)	3.265	3.265
Length/turn (m)	4.5	4.5
Number of channels	1875	1875
Saturation pressure psat (MPa)	0.891	0.003
Pressure drop (MPa)	0.1	0.11
Outlet temp. (K)	95	347
Typical ΔT (K)	11	30
Coolant exit velocity (m/s)	7.74	5.8

5. Vacuum Vessel

Scaling-up the Alcator C-MOD configuration has several implications to the vacuum vessel. The central transformer can be integrated with the vacuum vessel instead of the inner leg of the toroidal field coil, as in Alcator C-MOD. This added flexibility may have profound implications for the design of the vacuum vessel.

A reoccurring problem in the design of vacuum vessels is that in order to support adequately the disruption loads, the thickness of the vacuum vessel needs to be increased. Increasing the thickness of the vacuum vessel increases the disruption loads, and the thickness needs to be increased further. The limiting load in the inboard side of the vacuum vessel is due to buckling. A method to prevent this is to increase the strength of the vacuum vessel without substantially increasing its thickness. This can be achieved by placing ribs in the vacuum vessel. In order to minimize the space requirement, sections of the central transformer can be located inside the ribs.

Figure 8 shows a possible configuration. The poloidal field coil is integrated within the vacuum vessel. The ribs strengthen the vacuum vessel preventing buckling. The box-like structure of the vacuum vessel can be very strong. Furthermore, the vacuum vessel supports the axial loads of the poloidal field system. As presently envisioned, the vacuum vessel and the central solenoid are decoupled with respect to radial loads. The optimum coupling, however, still needs to be determined.

The design shown in Figure 8 is especially important for the large machine, since disruption loads are harder to support in this case.

The central solenoid conductor would be cooled internally, as shown in Figure 7. The cooling of the vacuum vessel and the first wall still needs to be addressed.

The vacuum vessel could be assembled and tested outside the machine and then inserted in one piece. For the larger machine, the weight of the vacuum vessel/central solenoid assembly may be too large. If this is the case, then poloidal sectors of the vacuum vessel (as opposed to toroidal sectors for BPX) could be lowered into the machine and then assembled in place. The inner vacuum vessel wall and central transformer can be handled as a single piece.

Rapid changes in the first wall and the divertor configurations can be achieved by constructing more than one vacuum vessel. In this manner one can be on the machine while another one is being refurbished. Reduced downtime for change-out would expedite the completion of the experiment. This is particularly important for the small hydrogen machine, since one of its missions is to study particle and energy flow handling.

Table IV

PF Parameters for Long Pulse
Operation of Hydrogen Machine

Maximum Energy Stored and Dissipated	
Stored energy (MJ)	95
Dissipated energy (MJ)	1180
Total energy (MJ)	1275
Maximum stored energy (MJ)	340
Maximum dissipated energy (MJ)	1250
Peak Power	
Magnetic power (MW)	69
Resistive power (MW)	31
Peak power (MW)	100
Flux Swing	
Start-up flux (V-s)	27.153
EOFT flux (V-s)	-17.847

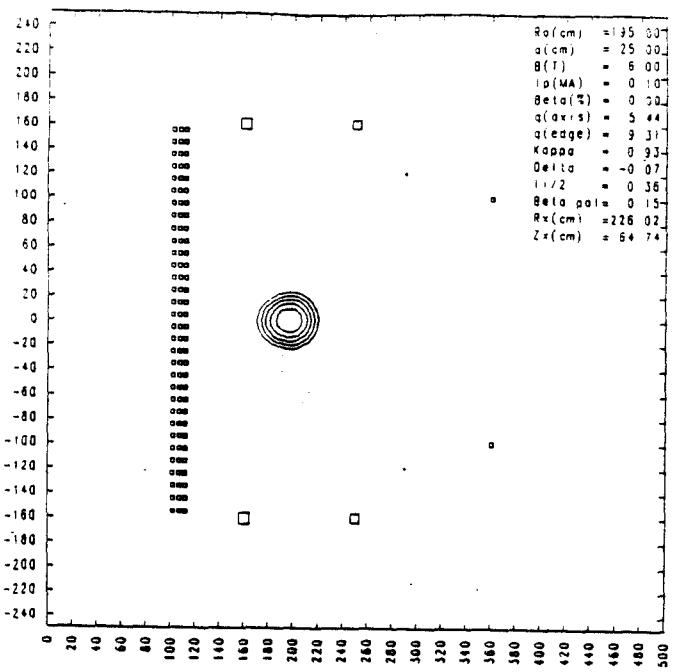

Figure 5a. Equilibrium at startup for the $R_0 = 1.95$ m, a = 0.65 m design.

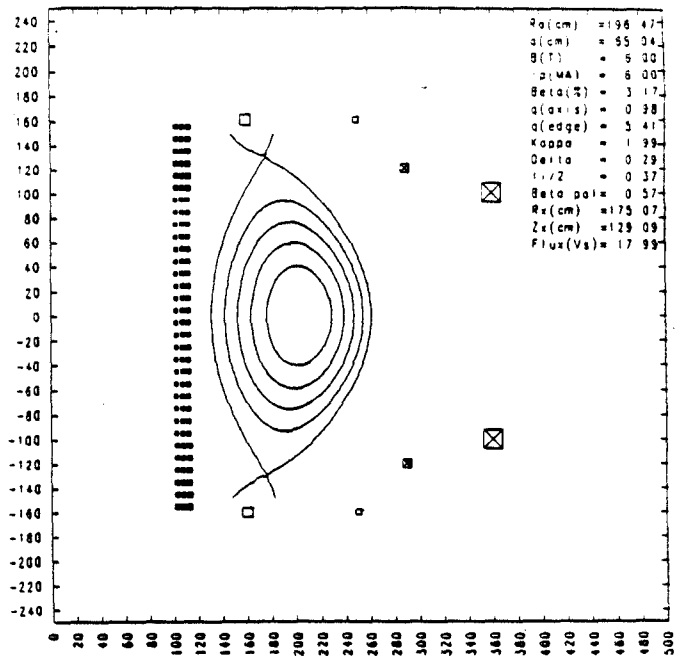

Figure 5b. Equilibrium at high β, end of flat-top for the $R_0 = 1.95$ m, a = 0.65 m design.

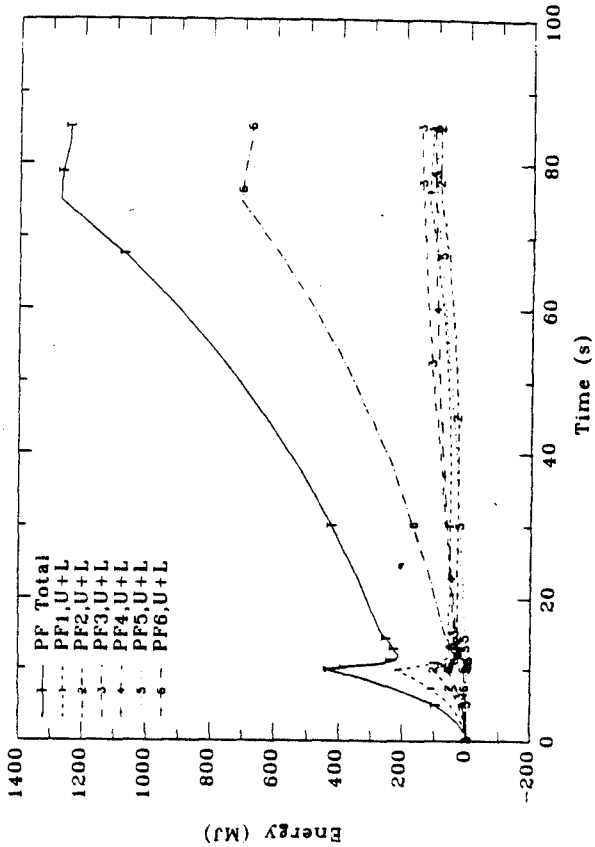

Figure 6a. PF field system characteristics for the $R_0 = 1.95$ m, a = 0.65 m design: (a) Energy (stored and dissipated).

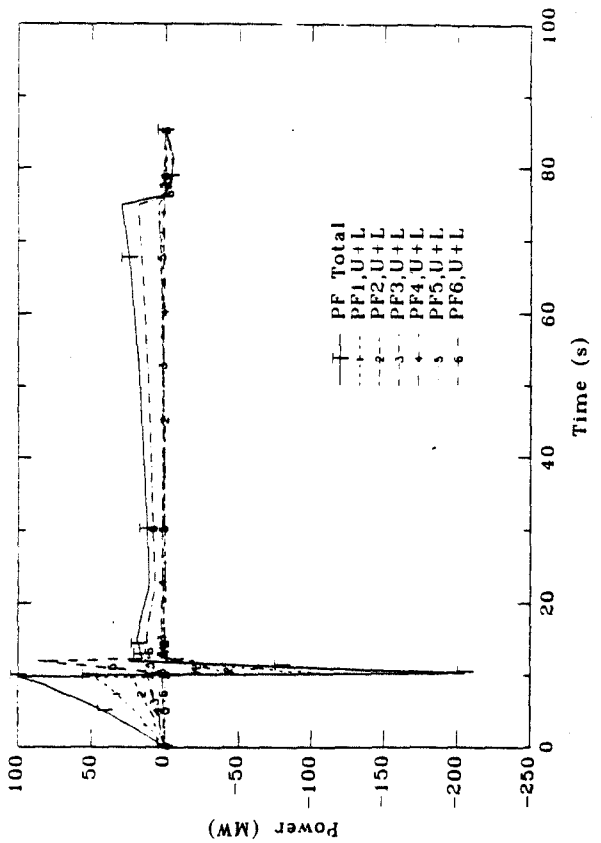

Figure 6b. PF field system characteristics for the $R_0 = 1.95$ m, a = 0.65 m design. (b) Power (magnetic and resistive).

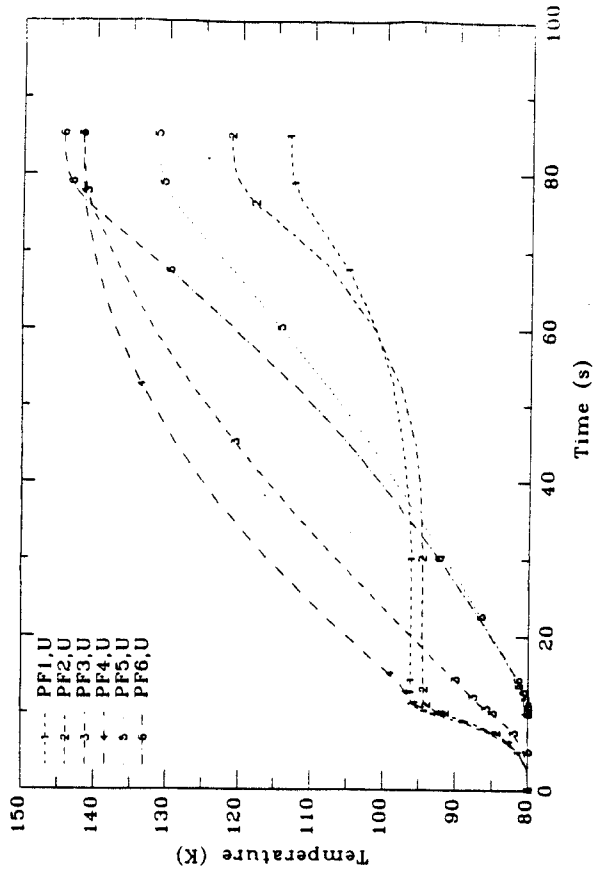

Figure 6c. PF field system characteristics for the R_0 = 1.95 m, a = 0.65 m design. (c) Coil temperatures.

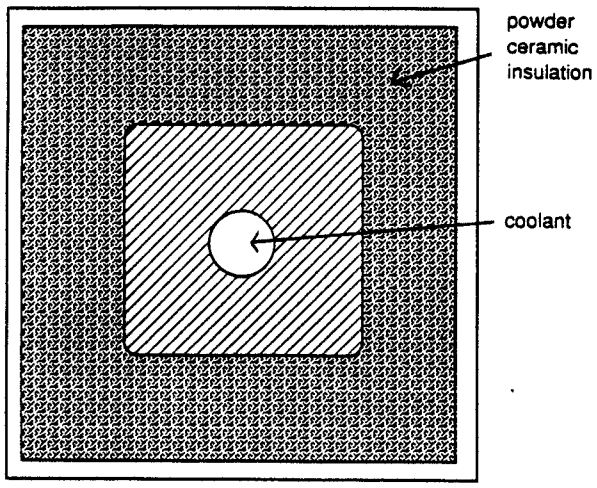

Figure 7. Poloidal field conductor cross-section.

This work was supported by the U. S. Department of Energy.

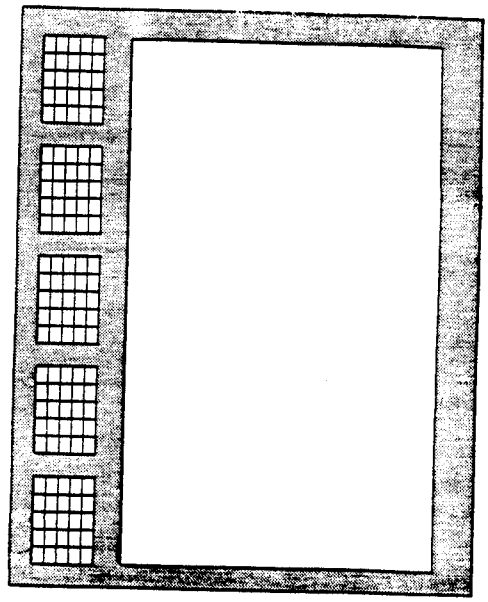

Figure 8. Integrated vacuum vessel/OH transformer configuration.

6. Summary and Conclusions

The use of demountable TF coils offers many advantages for tokamak experiments. Increased operational flexibility, due to the use of internal poloidal field coils, allows exploration of highly shaped plasmas. Also, the improved coupling efficiency between the plasma and the internal coils increases the allowable pulse length with inductive current drive. Long pulse operation can be explored, both in hydrogen and with DT.

The rapid disassembly and reassembly possible with demountable coils makes this type of coils very attractive for devices that will study particle and power handling, allowing fast access to first wall and divertor targets.

Areas that require additional work include the vacuum vessel and central solenoid assembly, detailed analysis of the sliding joints, further analysis of the internal poloidal field system and comparison with external ones, and cooling of the toroidal field coil. A reduced size demonstration plate, with ceramic insulation and cooling channels, is being planned.

References

[1] D. L. Jassby, Princeton Plasma Physics Lab. Report PPPL-1700 (1980).
[2] L. Bromberg, D. R. Cohn, and D. L. Jassby, Fusion Tech. **6** 597 (1984).
[3] R. J. LeClaire, R. E. Potok, L. Bromberg, et al., Fusion Tech. **8** 327 (1985).
[4] D. L. Jassby, R. A. Jacobsen, J. Kalnavarns, L. S. Masson, and J. P. Sekot, Princeton Plasma Physics Lab. Report 1809 (July 1981).
[5] I. H. Hutchinson et al., PFC/RR-88-11 (Aug. 1988).
[6] T. F. Yang, R. J. LeClaire, E. Bobrov, L. Bromberg, D. R. Cohn, and J. E. C. Williams, "A Demountable Copper TF Coil System for Ignition Test Experiments and Commercial Reactors, this conference.
[7] E. A. Chaniotakis, L. Bromberg, and D. R. Cohn, PFC/JA-91-5, Apr. 1991 (JFE, to be published).
[8] L. Bromberg, R. A. Krakowski, E. Cheng, D. R. Cohn, C. G. Bathke, and R. LeClaire, "Commercial Reactors with Resistive Magnets," this conference.

MAGNET DESIGN FOR THE ARIES-III D-He^3 REACTOR

L. Bromberg†, J. Schultz†, P. Titus‡, J.E.C. Williams†,
F. Najmabadi*, S. Sharafat*, and the ARIES Team

† Massachusetts Institute of Technology, Cambridge, Ma 02139
‡ Stone and Webster, Boston, Ma
* University of California, Los Angeles, Ca.

Abstract

The design options and the design integration of the magnet system for ARIES-III, a steady state reactor based on D-He^3, are presented. Both the toroidal and the poloidal field system are described. A new concept for manufacturing the toroidal field coil and for supporting the out-of-plane loads will be presented. The paper concentrates on those issues that are unique for the D-He^3 reactors.

1. Introduction

The ARIES-III reactor design study evaluates a D-He^3 tokamak reactor.[1] In this paper the implication on the magnet systems is described.

The toroidal field system is based on Nb_3Sn, with Nb-Ti in the lower field regions. Grading of the conductor and the structure is accomplished by a shell-type winding operation that minimizes the number of joints, increases the rigidity of the coil against out-of-plane loads, and simplifies the winding operation. The toroidal field coil size is minimized by the use of ripple-minimizing ferritic steels in the shield.

A major feature of the ARIES-III reactor is the possible need for inductive startup. Since during the burn most of the current is generated via bootstrap current, for ARIES-III the inductive requirements are dominated by the startup process. In order to compare the inductive startup to the non-inductive, the implications of inductive startup on the poloidal field system have been evaluated. This requirement places large constraints on the poloidal field system.

Operation in the second stability regime requires coils for stabilizing the kink modes. Helical coils, each segmented electrically in several places, and each independently driven, are required. These coils have to be located inside the toroidal field coil. Saddle-type coils have been designed to perform this function.

In Section 2, the design of the toroidal field coil is described. The structural analysis of the TF coil is presented in an accompaying paper [2]. Section 3 addresses the toroidal field ripple induced by the toroidal field coil, as well as methods of reducing the ripple produced by the compact ARIES-III coils. Section 4 describes the properties of the poloidal field system. Finally, Section 5 summarizes the results and identifies areas where additional work is needed.

2. Toroidal Field Coil

The design of the toroidal field coil follows the details of the ARIES-I toroidal field coil [3,4]. The coil is graded, with the highest field turns made of ternary Nb_3Sn (using the better properties of the conductor made via the powder metallurgy technology) while the lower field turns are made of NbTi. Incoloy 908 has been selected as the structural material. Cu-Nb has been used as the stabilizer and quench protection material.

The ARIES-III magnet, similar to previous magnets[5] and magnet designs[6] utilizes a winding method that eases the fabrication of the magnet by removing the stiffest material from the winding process. Thus, rather than winding all of the materials in the magnet, only the conductor requires winding. However, there are several disadvantages with the winding method used in these magnets. Each plate needs as many joints as there are grades of the superconductor. ARIES-I, with 5 grades, 16 coils, and 24 plates per coil, has about 2000 joints. This large number of joints is troublesome due to both electrical and cryogenic reliability. A second disadvantage of the approach is that the conductor/plates offer very little out-of-plane support. The out-of-plane load has to be transferred to the caps and the bucking cylinder. It is hard to lay the conductors in the slots in the plates; this process requires a three-dimensional winding process.

For ARIES-III, an innovative winding method is utilized that winds the conductor in structural shells, instead of plates. The arrangement in this new configuration is shown in Figure 1. Shells are nested in such a way that the conductors serve as keys between adjacent shells. The depths of the grooves in the shells are determined by the design of the conductor so a different depth is required for each grade. In this way, large out-of-plane strength is obtained, since the shells are prevented from sliding with respect to each other. The structural advantages of this configuration are described in an accompanying paper.[2] By layer-winding the magnet, the multitude of joints needed in pancake-wound-graded configuration, as in ARIES-I, is avoided. This simplifies not only the electrical connections in the magnet, but also the cryogenic connections. The winding process is also simplified, since inserting the conductor inside the outer slot in the shell requires a simple one-dimensional operation. After winding a conductor layer, the next shell is located in place. To allow assembly of the magnet, the shells have a slot, probably in the outer regions of the magnet. After locating it in place, the structural continuity of the shell may be achieved by carefully welding the shell in place (with the use of a lip-weld to prevent damage to the superconductor under the shell weld).

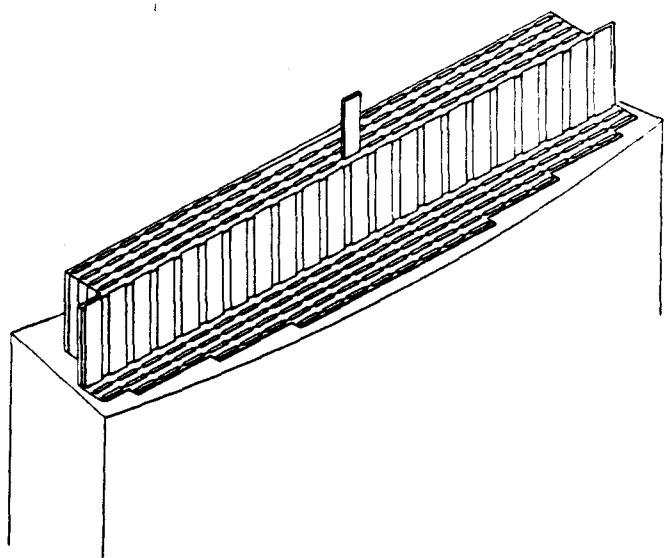

Figure 1. Shell-type geometry for alternative layer wound concept.

Alternatively, the large space available in the outer regions of the magnet could be utilized for mechanically joining the edges across the slot of the shells.

Coil design parameters are shown in Table I. I_{pack} is the conductor current, V_{max} is the voltage limitation during quench, and $S = \int j^2 dt$ (determines the heating in the conductor resulting from a quench). The conductor grading information is shown in Table II. In this table $Ar_{superconductor}$ is the superconductor cross sectional area, $Ar_{stabilizer}$ is the stabilizer cross sectional area, $Ar_{conductor}$ is the conductor total cross sectional area, Ar_{Helium} is the cross sectional area filled with He, Ar_{wall} is the cross sectional area of the structure, $Ar_{insulation}$ is the cross sectional area of the insulation, and Ar_{total} is the total cross sectional area of the given grade. h_{cond} and w_{cond} are the conductor height and width, t_{wall} is the thickness of the structural wall, $s_{toroidal}$ is the total toroidal thickness of the turn, and r_{radial} is the radial thickness of the rows. The two first grades are Nb_3Sn and the other two are NbTi.

The design results are shown in Table III. B is the peak field for the row of conductor, r_{inner} and r_{outer} are the inner and outer radii of the respective row (including structure), and σ_{rad} and σ_{tot} are the radial and Tresca stresses for the row of conductors. The number of columns refers to the number of conductors in the toroidal direction for the given row. The inner leg cross section of the optimized design is shown in Figure 2.

3. Ripple Considerations

The ripple in ARIES-III, as with any high temperature device, needs to be controlled in order to minimize the losses of the fast fusion products.

Figure 3 shows contours of constant peak-to-average ripple in the region of interest for the ARIES-III design in the absence of shimming. For ARIES-III, a magnetic steel, HT-9, is being proposed for the shield. The use of magnetic material inside the toroidal field coil opens the possibility of using ferromagnetic shimming of the toroidal field ripple. The Curie temperature of HT-9 ranges from 500 to 700 °C, and it has been assumed that the temperature of the shield is below the Curie temperature.

Calculations of optimum placement of magnetic material for cancelling the ripple would proceed as follows: the ripple shown in Figure 3 in the domain of interest is Legendre-expanded.

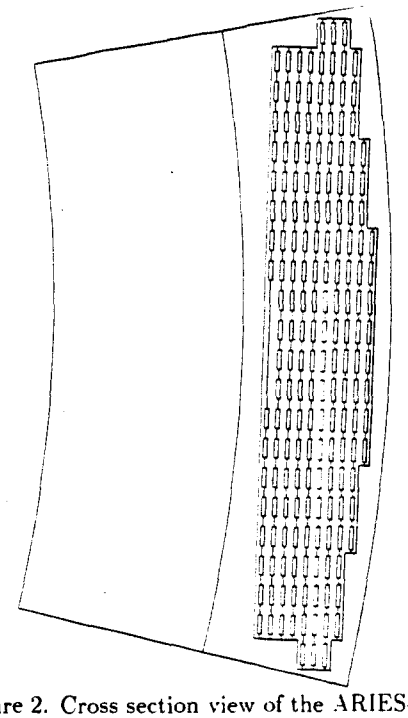

Figure 2. Cross section view of the ARIES-III TF coil

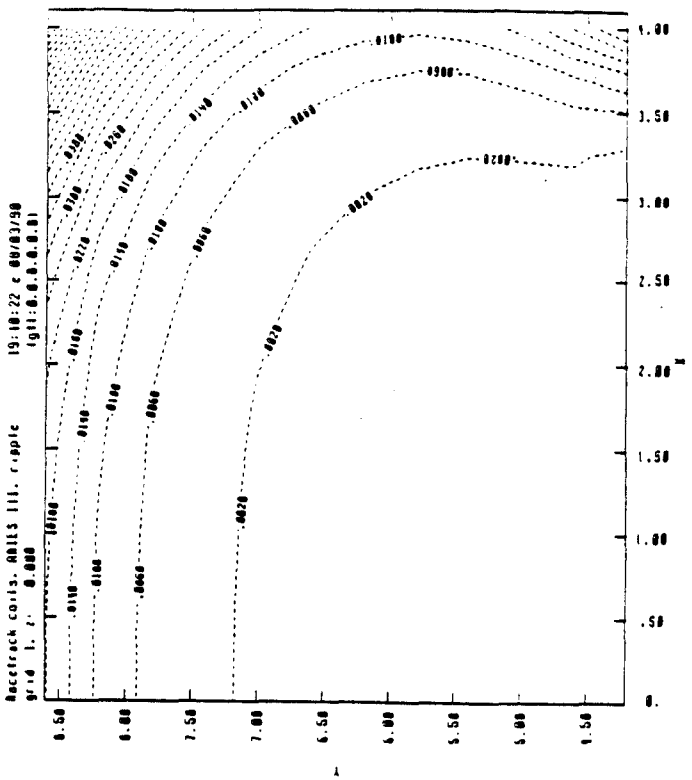

Figure 3. Ripple in ARIES-III in the absence of the ripple minimization from the magnetic shield.

Table I. TF coil design parameters

Parameter	Design value
Toroidal field (T)	7.8
Major radius (m)	7.4
Maximum toroidal field (T)	14.4
Energy stored per circuit (GJ)	1.7
Total stored energy (GJ)	56
I_{pack} (A)	100000
V_{max} (kV)	20
S_{max} (A^2s/m^4)	5×10^{16}
Number of coils	16
Number of grades	4
Thermal contraction (293 K to 4 K)	
superconductor	-4×10^{-4}
stabilizer	5×10^{-4}
plate	-4×10^{-4}
case	6×10^{-4}
insulation	-4×10^{-4}
j_{cond} (MA/m^2)	240
j_{magnet} (MA/m^2)	40.2

The various harmonics of the ripple disturbance are thus derived. A ferromagnetic dipole produces an infinite number of harmonics. However, by placing a finite number of ferromagnetic dipoles in the space surrounding the domain of interest, we can create harmonics equal in magnitude and opposite in sign to the harmonics produced by the ripple disturbance. This technique is widely used for ferromagnetic shimming of magnets for nuclear magnetic resonance spectroscopy and imaging, where it is possible to decrease inhomogeneities of 10^{-3} to below parts per million.[7] At the Francis Bitter National Magnet Laboratory at MIT, a 600 MHz spectrometer (14.2 T) and the 60 cm bore 2T MRI have been successfully shimmed.[7]

Table II. Conductor design parameters

grade	1	2	3	4
Maximum field (T)	3.9	7.5	11	14.6
j_c (10^8A/m^2)	47	78	31	11
T_c (K)	6.65	5.02	11.06	8.69
$Ar_{superconductor}$ (10^{-4}m^2)	0.21	0.12	0.31	0.89
$Ar_{stabilizer}$ (10^{-4}m^2)	3.54	3.54	3.54	3.54
$Ar_{conductor}$ (10^{-4}m^2)	3.75	3.67	3.86	4.43
Ar_{Helium} (10^{-4}m^2)	0.51	0.50	0.51	0.54
Ar_{cs} (10^{-4}m^2)	4.27	4.18	4.38	4.97
Ar_{wall} (10^{-4}m^2)	12.7	12.5	12.1	11.7
$Ar_{insulation}$ (10^{-4}m^2)	1.9	1.89	1.87	1.89
Ar_{total} (10^{-4}m^2)	18.8	18.6	18.3	18.6
h_{cond} (10^{-2} m)	0.995	0.952	0.954	0.96
w_{cond} (10^{-2} m)	4.29	4.39	4.59	5.18
t_{wall} (10^{-2} m)	1.25	1.21	1.06	0.806
$s_{toroidal}$ (10^{-2}m)	7	7	7	7
r_{radial} (10^{-2} m)	2.7	2.7	2.7	2.7
structural fraction	0.94	0.96	0.91	0.79

Table III. Row by row design parameters

Row	1	2	3	4	5
Grade	4	4	4	4	3
B (T)	14.47	13.97	12.94	11.42	9.71
r_{inner} (m)	4.06	4.04	4.01	3.98	3.96
r_{outer} (m)	11.32	11.35	11.37	11.40	11.43
σ_{rad} (MPa)	88	170	250	310	280
σ_{tot} (MPa)	641	722	794	862	832
Number of columns	8	14	20	22	22

Row	6	7	8	9	10
Grade	3	2	2	1	1
B (T)	7.99	6.23	4.62	2.99	1.34
r_{inner} (m)	3.93	3.90	3.88	3.85	3.82
r_{outer} (m)	11.45	11.48	11.51	11.53	11.56
σ_{rad} (MPa)	310	300	310	310	310
σ_{tot} (MPa)	862	844	862	862	862
Number of columns	22	20	20	20	16

Alternatively, the thick shield could be used for the shimming of the toroidal field. In either case, non-uniformities of the shield (due to openings, gaps between shield sectors, etc.) would result in additional ripple and needs to be included in the calculations.

The ferromagnetic material is saturated, but the remaining induction is used for the shielding. An important effect which should also be considered is the magnetic forces on the shield due to the gradient in the field (both due to the vacuum field and because the magnetization changes if the temperature is not uniform).

Due to lack of resources, the ripple cancellation calculations were not completed. However, there is sufficient flexibility by the use of the thick shield, by the choice of the shield temperature, and by the placement of irregular sections of ferromagnetic material to reduce the ripple to acceptable levels.

4. PF Coils

In this section the PF coil set is described. In ARIES III, in addition to the poloidal field coils required for MHD equilibrium, a set of helical coils is required for MHD stability.

The PF coils in ARIES-III, as in ARIES-I, are external to the TF system and are superconducting, using internally cooled, cable-in-conduit conductor. The conductor is similar to the TF conductor. The design of the poloidal field (PF) magnet system is, however, more demanding than for ARIES-I due to the larger plasma current in ARIES-III and the need for inductive plasma startup.

The PF system is designed to induce and control the 28 MA plasma over a range of beta and internal inductance. In order to determine the tradeoffs with RF-driven, noninductive plasma startup, the poloidal field system has been designed to provide full ohmic initiation. Since there is no quantitative flat-top requirement, the design criterion was to stay within the flux swing regime in which cost increases very slowly with capability. The PF coil set is described in Table IV.

An inductive capacity of 480 V-s was selected. This includes a capability of inductive plasma startup and flat-top at full current for either high-beta or low-beta plasmas in order to ensure the ability to heat and quench the burning plasma.

In order to optimize a poloidal field system that requires substantial flux swings, it is necessary to determine the optimum flux bias. A scenario code has been modified to estimate the optimum bias in ARIES-III. The scenario is specified at a small number of discrete times. The equilibria and associated coil currents at these times are calculated at two different values of flux linkage. With that information, it is relatively easy to extrapolate the coil currents to any flux linkage. The discrete times during the discharge are initiation, low β, and high β.

The scenario code is then utilized in order to design the poloidal field system. The coil size and the composition (structural material, conduit, superconductor, stabilizer, helium, and insulation fraction) are determined by the most demanding condition at any of the the three points during the scenario. The process is repeated several times for varying initial flux linkage (bias) until a relatively optimized poloidal field system is obtained. The optimization process consists of minimizing the cost of the system.

In order to calculate currents and forces in the coils after disruptions, the simplifying assumption is made that the coils are connected to low impedance power supplies. The flux-conserving currents in each coil due to disruptive disappearance of the plasma current are calculated. The radial and axial force influence matrices are then used to calculate the forces on each coil at each moment of time, following a flux-conserving disruption. The radial force is converted to an average tensile stress over the winding pack cross section, while the axial force is converted to an average axial compression stress over the coil bearing area.

Guidance is given to the selection of power supplies by monitoring when each coil current and voltage have the same polarity, and recording the maximum individual voltage and current for each polarity.

Results of the optimization are shown next. The peak field in the PF system is only 12.8 T, as shown in Figures 4 a and b. These figures show the maximum field at the coils for the cases of initiation and high beta as a function of the bias flux swing. In order to provide the approximately 500 Volt-s that are required for inducing the plasma current, the flux swing needs to go from 165 at startup to -320 at the start of high beta flat-top.

The feasibility parameters for the different coils at the high-β are shown in Table V. In this table, B_{max} is the maximum field, $f_{c,max}$ is the fraction of critical current, f_{Jprot} is the fraction of maximum protection current, T_{head} is the minimum temperature head room, E_{head} is the minimum energy head room, f_{ftr} is the transition fraction, $\sigma_{Tr,ext}$ is the maximum Tresca stress, and $\sigma_{t,mem}$ is the maximum membrane stress. Similar tables are generated for the other points in the scenario, and the coil composition and size is varied until all the critical parameters are within the feasible and acceptable range.

Table IV. ARIES PF system winding pack dimension

Coil	R (m)	Height (m)	dR (m)	dZ (m)
PF1,U,L	2.73	±0.99	0.76	0.51
PF2,U,L	2.73	±1.67	0.76	0.76
PF3,U,L	2.77	±3.61	0.65	0.65
PF4,U,L	5.57	±6.58	0.87	0.87
PF5,U,L	6.82	±6.74	0.43	0.43
PF6,U,L	8.64	±6.46	0.72	0.72
PF7,U,L	12.56	±3.05	0.97	0.97

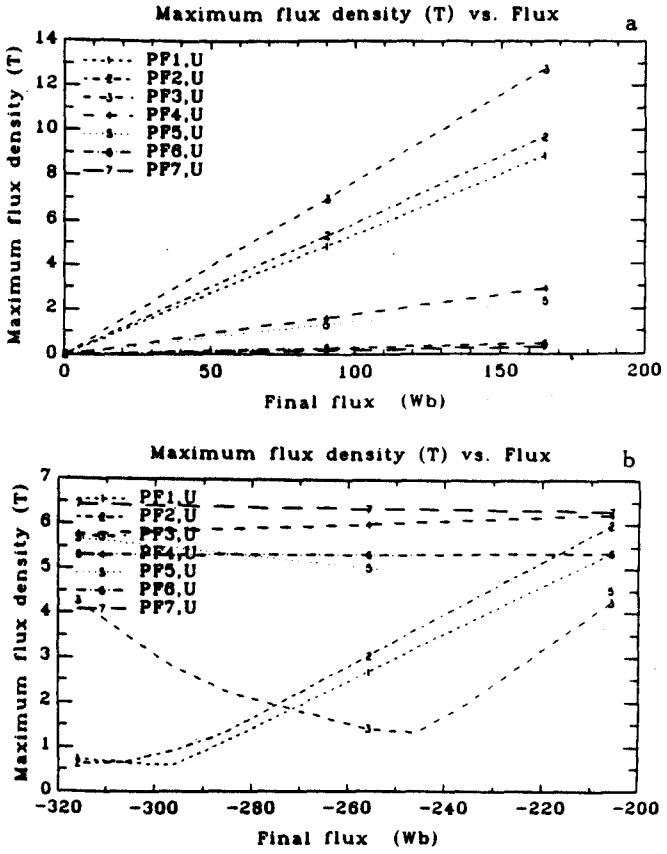

Figure 4. Maximum flux densities in each PF coil: a) initiation; b) high β.

Surprisingly, the peak PF energy is a modest 16.5 GJ, dominated by the high-beta plasma requirements. This number is comparable to that of ITER. Because of the slow charging of the coils, the peak power and power supply requirements are modest.

The design approach to ARIES-I was that the magnet should be able to absorb the losses, forces, and voltage transients from a disruption at any time during a startup or shutdown. The implications of off-normal conditions on the poloidal and the toroidal field system have not been evaluated. Due to the larger plasma current, the effects are expected to be harder to deal with than in ARIES-I.

5. Summary

The critical issues of the toroidal and the poloidal systems for ARIES have been presented in this paper. The impact of the use of D-He^3 fuel in the ARIES-III magnets are:

- the ferritic shield, allowed due to the reduced neutron activation with D-He^3, can be used to decrease the toroidal field ripple, minimizing the size of the toroidal field coils.
- D-He^3 decreases the shielding requirement to the magnet, further decreasing the overall size of the device. However, shield minimization for normal operation raises cryogenic cooling issues during the DT start up (from the increased neutron loading). It has been determined that sufficient thermal inertia in the liquid helium permits relatively long transient heating (on the order of minutes).
- Operating deep in the second stability regime requires the use of helical coils for kink mode stabilization. The design, maintenance, and operation of such coils presents difficult challenges.
- Inductive startup increases the cost of the PF system, but only moderately. The PF cost for a fully inductive startup is only 100 M$.

The toroidal field magnet, due to the intermediate value of the toroidal field, is not particularly aggressive. A novel scheme for improving the structural, electrical, and cryogenic behaviour of the plate magnets has been studied.

The poloidal field (PF) magnet system is substantially more aggressive than that of ARIES-I. The helical coils required for MHD kink stability control present a difficult challenge. The helical coils are described in an accompanying paper.[8] The rest of the poloidal field system coils (the ones that provide for MHD equilibrium) are external to the TF system.

The pulse losses due to interaction between the poloidal field and the toroidal field require further study. In particular, the effect of the pulse loads from the helical coils on the superconducting toroidal and poloidal field system needs to be studied. The power conditioning equipment to drive the helical coils also needs additional investigation. Off-normal loads (disruptions, coil failures) in the magnet system need to be investigated.

Table V. PF coil feasibility parameters

Coil	B_{max} (T)	$f_{c,max}$ ( )	f_{Jprot} ( )	T_{head} (K)	E_{head} (J/cc)	f_{ftr} ( )	$\sigma_{Tr,ezt}$ (MPa)	$\sigma_{t,mem}$ (MPa)
PF1,U	5.3	0.08	0.27	9.1	43.3	0.1	187	158
PF2,U	5.9	0.05	0.13	9.1	6.6	0.3	232	200
PF3,U	4.2	0.04	0.17	10.2	8.0	0.1	124	108
PF4,U	6.2	0.55	1.73	4.2	46.4	0.6	660	0
PF5,U	5.6	0.57	0.66	4.2	11.7	0.0	658	651
PF6,U	5.3	0.59	1.61	4.0	36.0	0.4	697	684
PF7,U	6.4	0.59	2.69	3.7	35.5	0.9	671	654

References

[1] F. Najmabadi, et al., "ARIES-III Tokamak Reactor Study," elsewhere in this conference.

[2] L. Bromberg, P. Titus and J.E.C. Williams, "Nested Shell Superconducting Magnet Design for Commercial Tokamak Reactors," presented in these proceedings.

[3] J. Schwartz, L. Bromberg, D.R. Cohn, and J.E.C. Williams, "A Commercial Tokamak Reactor Using Super High Field Superconducting Magnets", *Fusion Tech.* **15** 957 (1989).

[4] L. Bromberg, D.R. Cohn, J. Schultz, J. Schwartz, P. Titus, J.E.C. Williams, S.P. Grotz, R.L. Creedon, and C.P.C. Wong, "Magnet Design for the ARIES-I High Field Tokamak Reactor," *Fusion Tech 1990*, BV. E. Keen, M. Huguet, R. Hemsworth, *eds.*, Elsevier Science Publishers B.V., (1991).

[5] D. S. Beard, W. Klose, S. Shimamoto, and G. Vecsey, *eds.*, "IAEA Large Coil Task; Chapter 3: Characteristics of the Coils," *Fusion Eng. & Des.* **7** 23 (1988).

[6] J. H. Schultz, F. S. Malick, D. R. Cohn, and J. E. C. Williams, "High Field Compact Tokamak Reactor," in *Proc. 8th Symp. of Fusion Research* (1979).

[7] E. Bobrov, Francis Bitter National Magnet Laboratory, Cambridge, Ma, private communication.

[8] C. Kessel, et al., presented in these proceedings.

This work was supported by the U. S. Department of Energy Contract No. DE-FG02-91ER-54110.

NESTED SHELL SUPERCONDUCTING MAGNET DESIGNS

L. Bromberg, P. Titus°, and J. E. C. Williams

Massachusetts Institute of Technology
Cambridge, MA 02139
°Stone and Webster, Boston, MA 02215

Abstract

A new concept for manufacturing the toroidal field coil is described. Instead of structural plates, the magnet is wound in interlocking shells. The magnet configuration is described and the advantages explored. Structural analysis of the concept is performed using the ARIES tokamak reactor parameters. The effectiveness of a structural cap, placed above and below the toroidal field coils and used only to balance opposing torques generated in different places of the coil, is quantified.

1. Introduction

A novel concept of winding toroidal superconducting magnets is described. Previous monolithic-like magnet designs[1,2,3] utilize a winding method that eases the fabrication of the magnet by removing the stiffest material from the winding process. In these designs the conductor (superconductor and copper) is wound in grooves machined in the structural material. The resulting pancakes are in the shape of plates, increasing reliability and stiffness for in-plane loads.

There are several disadvantages with the winding method used in these magnets. If grading is used, each pancake needs as many joints as there are grades of the superconductor. ARIES-I, with 5 grades, 16 coils, and 24 plates per coil, has about 2000 joints. This large number of joints is troublesome due to both electrical and cryogenic reliability. A second disadvantage of the approach is that the conductor/plates offer very little out-of-plane support. The out-of-plane load has to be transferred to the caps and the bucking cylinder. And lastly, the winding process is complex. It is hard to lay down the conductors in the grooves in the plates; this process requires a three-dimensional winding process.

Reaction of the out-of-plane loads in tokamak reactors is a difficult problem. This is due to the fact that the designs are such that the winding pack, which forms a large section of the coil, cannot carry any of the loads. The use of plates allows the use of the conductor as a structural member for in-plane loads, but the pancakes do not have any stiffness to react the out-of-plane loads.

In this paper, a novel concept of the toroidal field magnet configuration is described. In the nested shell concept, the conductor is layer-wound in grooves in a shell that lies in the toroidal direction. This simplifies substantially the winding process, both in laying down the conductor and in reducing the number of joints in the graded case. An entire row (of the same grade) is wound on the shell. The minimum number of joints per coil would be equal to the number of grades.

The characteristics of the novel winding operation is described in this paper. Section 2 describes the concept; Section 3 analyzes some of the options available through this scheme; Section 4 describes the detailed stress analysis; and, finally, Section 5 summarizes the results and identifies areas of future work.

2. Magnet Configuration

An innovative winding method, the "nested shell" concept, is proposed that winds the conductor in structural shells, instead of plates. The arrangement in the novel configuration is shown in Figure 1.

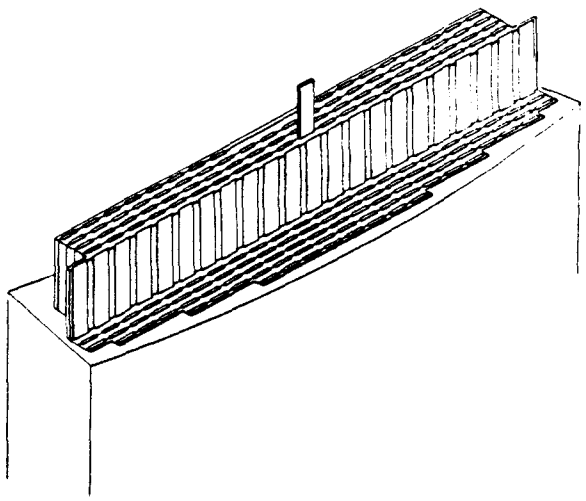

Figure 1. Shell-type geometry for alternative layer-wound concept.

The conductor is laid down in grooves in toroidal shells. The grooves are thinner than the conductor. The shells are nested in such a way that the conductors serve as keys between adjacent shells, interlocking them. A monolithic-like structure can be constructed in this manner. Large out-of-plane stiffness is obtained, since the shells are prevented from sliding with respect to each other. The structural advantages of this configuration will be described in Section 4.

By layer-winding the magnet, the multitude of joints needed in pancake-wound graded configuration, as in ARIES-I, is avoided. This simplifies not only the electrical connections in the magnet, but also the cryogenic connections. The winding process is also simplified, since inserting the conductor inside the outer slot in the shell requires a simple one-dimensional operation. After winding a conductor layer, the next shell is located in place. To allow assembly of the magnet, the shells have a slot, probably in the outer regions of the magnet. After locating it in place, the structural continuity of the shell may be achieved by carefully welding the shell in place (with the use of a lip-weld to prevent damage to the superconductor under the shell weld). Alternatively, mechanical joints can be used if the slot in the shell are in the outer leg of the magnet.

The depths of the grooves in the shells are determined by the design of the conductor[3,4], so a different depth is required for each grade. The grooves of the shells are half as deep as the conductors are thick. Adjacent shells have matching grooves, and the conductors fit in both sets of grooves. That way the conductor interlocks adjacent shells.

Coils wound in this fashion behave as monoliths in the toroidal and the out-of-plane directions, with substantial out-of-plane load carrying capability. The simplified model shows that the concept can minimize the structure required to handle the out-of-plane loads.

The out-of-plane structure to be studied is similar to that proposed for ARIES-I. Structural caps on the top and bottom sections of the coils are used to balance opposing torques generated in different regions of the coils. The caps are free-floating and are not attached to either the bucking cylinder or the building.

3. Magnet Options

With the layer winding/shell configuration of the toroidal field coil, it is possible to increase the toroidal width of the coils, providing large increases in load-carrying capabilities. This is shown schematically in Figures 2 and 3. Only the conductor of one of the shells is shown in these figures. This arrangement is difficult to accomplish with plate-type pancakes[1,2,3] or in pancake-wound coils, as in ITER. In the case of the plate supporting magnet, the plates would have varying thicknesses, which raise difficult manufacturing issues.

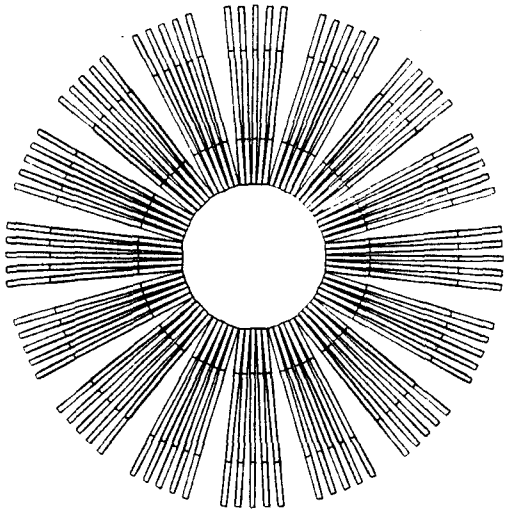

Figure 2. Elevation view of configuration of shell-type toroidal field coil with varying toroidal coil thickness. Only conductor is shown.

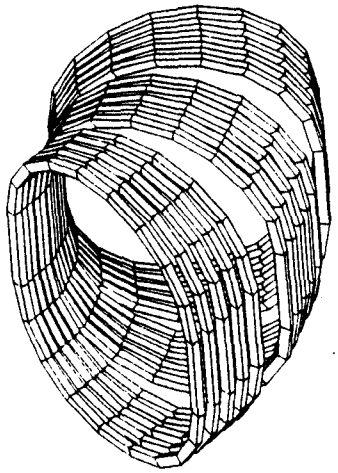

Figure 3. Top view of configuration of shell-type toroidal field coil with varying toroidal coil thickness. Only conductor is shown.

The shells will have to be made with varying widths in the toroidal direction. Good manufacturing techniques are required in order to provide for proper fitting as the shells are wrapped around the conductor. Alternatively, the shells can be manufactured in situ by a process of wrapping fibers into the poloidal direction, with matrix materials deposited after the fiber-winding process. Two-dimensional fiber mats or metal sheets could be interleaved with these fibers to give both very large moduli in the poloidal direction, and stiffness in the toroidal direction.

Enlarging the width of the coils may interfere with maintenance and access. For the ARIES magnets, maintenance involves removing a sector with associated TF coils. Therefore, enlarging the width of the coils would not affect maintenance of the first wall or blanket.

With the use of the nested shells, it is possible to vary the amount of structure in a given turn of the magnet by simply adjusting the thickness of the shell. In effect, the smeared current density (average current density in each turn including structure, conductor, and void) of the coil can be adjusted, even though the current per turn is held constant. Those areas that would experience larger loads can be reinforced structurally.

The same technique may be used in order to vary radially Young's moduli of the different shells. The moduli of different turns of the magnet may be adjusted to distribute stress more uniformly or to obtain the desired coil shape. The variation in moduli can be done relatively easily by using fiber-reinforced structural materials. By simply adjusting the ratio of matrix to fiber, the modulus of a shell can be adjusted. In this manner, coils with a radially constant factor of safety (ratio of allowable stress to actual stress) can be obtained without large implication to the shape of the coil. If this were not the case, the Princeton-D coil shape would result, since it is the natural shape of a coil in the absence of intercoil structure.

In both the cases of varying the thickness of the structural material and the moduli of the shells, the properties of the coil will be constant along the turns, but vary across turns.

4. TF Coil Structural Considerations

A structural analysis similar to ARIES-I[3] was carried out. The cyclically symmetric ANSYS model consists of a wedge which represents 1/16th of the machine. It is also symmetric about the equatorial plane. The parameters for the toroidal field coil follow the detailed optimization of the magnets for ARIES[3]. Some of the main parameters of the ARIES magnets are shown in Table I.

Table I

TF Coil Design Parameters
Used for the Present Calculations

Parameter	Design Value
Toroidal field (T)	13
Major radius (m)	6.5
Maximum toroidal field (T)	21
Energy stored per circuit (GJ)	4.1
Total stored energy (GJ)	130
Number of coils	16
j_{cond} (MA/m^2)	155
j_{magnet} (MA/m^2)	27

The ANSYS code was used to analyze the three-dimensional behaviour of the shell-type concept in the absence of the structural caps used in the ARIES-I design. The purpose of the structural caps in ARIES-I is to balance large and opposite out-of-plane loads produced in the horizontal legs of the coils, without transferring them to the bucking cylinder or to external structures. The advantage of not using the structural caps would be increase access to the shield and divertor regions, and easier maintenance and assembly of the reactor. The near-monolithic behaviour of the legs of the toroidal field coils could be utilized to transmit the out-of-plane loads to the bucking cylinder. The normal load condition case was analyzed. Off-normal conditions, representing single or multiple toroidal field coil failures and disruptions, among others, remain to be studied.

Figure 4 shows the finite element models for the cases with (a) and without (b) the structural caps. The toroidal field coil leans against a bucking cylinder. The toroidal field coil and the bucking cylinder are attached by keys running along their length in order to assure transmission of the out-of-plane loads. Gaps are inserted between toroidal field coils to assure that the coils do not wedge against each other. The cross-section of the coil is kept constant. Elements have been introduced between the toroidal field coil and the bucking cylinder to prevent the transmission of vertical loads from the toroidal field coil to the bucking cylinder. In practice, friction will transfer some of the vertical tension in the coil to the bucking cylinder, decreasing the loads in the toroidal field coil and increasing the loads in the bucking cylinder.

Figures 5(a) and 5(b) show the equivalent von-Mises stresses on the toroidal field coil for the case with (a) and without (b) the structural caps. The values of the stresses are in MPa. The average vertical stresses in the throat of the toroidal field coil on the midplane are about 500 MPa. The radial stresses are ~140 MPa. The equivalent average stress on the midplane, with all the loads added, is about 600 MPa. Accounting for space for gaps, cooling and insulation, the average equivalent stresses (von-Mises) in the toroidal field coil are about 700 MPa. The peak stresses in the horizontal leg of the toroidal field coils are reduced by about 500 MPa due to the action of the structural caps. This shows the effectiveness of using the free floating caps. As will be shown below about 300 MPA of the increase is due to increased shear loads, and the other 200 MPa is due to the removal of the section of the structural shell that acts as a bucking post, increasing the coil tension by about 200 MPa.

The stresses in the external structure are shown in Figures 6 (a) for the case with structural caps, and 6 (b) for the case without structural caps. The stresses in the bucking cylinder for both cases are approximately the same. Peak stresses in the caps are about two-thirds of the stresses in the toroidal field coil in the absence of the caps.

The distribution of shear stresses is shown in Figures 7 (a) and (b) for the cases with and without the structural caps, respectively. The calculations were performed for the high-β equilibria described in reference 5. The τ_{xy} shear stresses are shown, where x is the radial direction and y is the vertical direction. The shear stresses in the case with the structural caps are decreased by about 300 MPa. The τ_{xy} shear stresses account for about half of the increase in the von-Mises equivalent stresses shown in Figures 5 (a) and (b). Even though the structural caps are not connected to any external structure and therefore cannot react a net torque, it is very effective in balancing opposing torques generated in different sections of the TF coils.

The allowables for the structural materials used in the toroidal field magnet are a membrane stress of 900 MPa and membrane plus bending of 1800 MPa. The stresses in the region where the vertical leg ceases to be supported by the bucking post are close to the allowable. This is a consequence of a poor choice of the height of the bucking cylinder in the finite element model in the case without the cap, as shown in Figure 6. The bucking cylinder is too short, leaving large sections of the inner region of the toroidal field coils unsupported. In addition to the increased shears due to the removal of the structural caps, the tension in the horizontal leg increases by about 200 MPa due to the removal of the support of the radial loads. Increasing the height will decrease both the in-plane tension and the out-of-plane stresses. A new model was constructed to take this into account, shown in Figure 8. Due to lack of resources, the calculations were not carried out to completion. However, rough estimates indicate that increasing the height of the bucking cylinder will decrease the stresses in the outer region of the magnet by about 20%, bringing those regions below the allowable. An additional advantage of increasing the height of the bucking cylinder is the lowering of the stress concentration in both the TF coil and the bucking cylinder in the discontinuity area where the bucking cylinder stops. Finally, increasing the height of the bucking cylinder would decrease the hoop stresses in the bucking cylinder.

The results presented above are for normal loads. In order to assure that off-normal conditions can be supported, a structural cap similar to that of the ARIES-I design[3] has been allowed in the designs. The cap is substantially lighter due to the large capacity of the coils to support off-normal loads.

The deflections in the top and bottom sections of the structure are on the order of 0.2-0.3 m in the absence of the structural caps. The machine height is about 10 m high and the major radius location of the displacement is about 7 m. The relative displacements are therefore small. Although the displacements are large, the strains in the structure are small, with relative small shear and fiber stresses. The motion of the top and bottom sections is necessary in order to load the bucking cylinder to react the out-of-plane loads.

Further work needs to be done in order to determine the behaviour of the toroidal field coil under off-normal conditions (disruptions, coil failures, etc.).

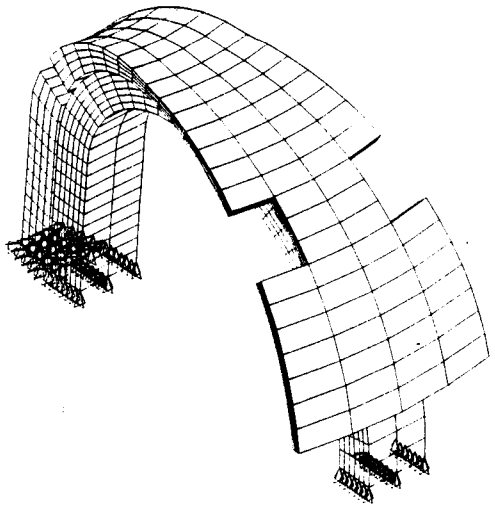

Figure 4a. Finite element model of the ARIES-III TF coil and supporting structure with structural caps.

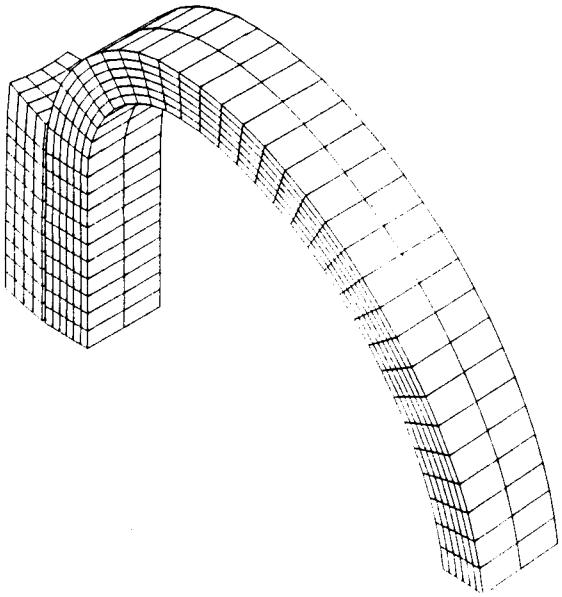

Figure 4b. Finite element model of the ARIES-III TF coil and supporting structure without structural caps.

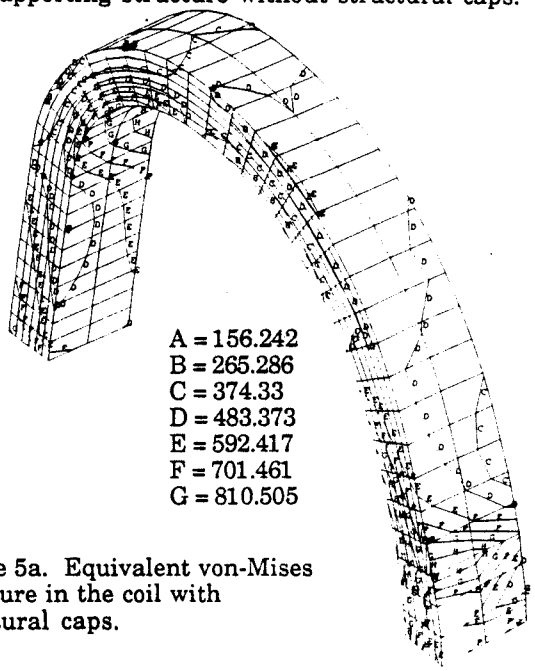

Figure 5a. Equivalent von-Mises structure in the coil with structural caps.

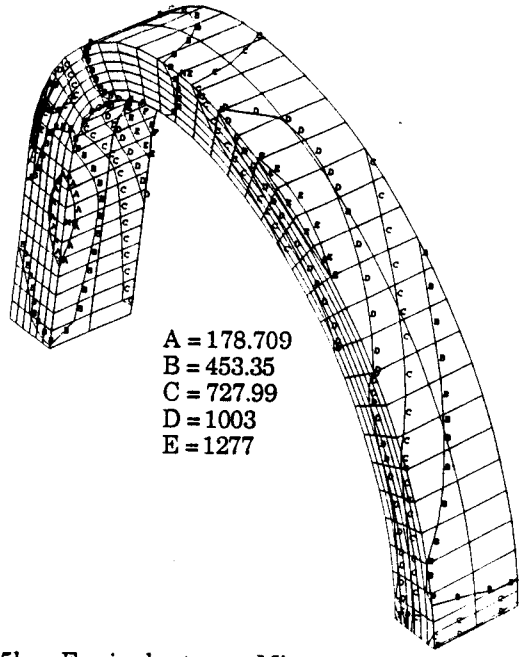

Figure 5b. Equivalent von-Mises structure in the coil without structural caps.

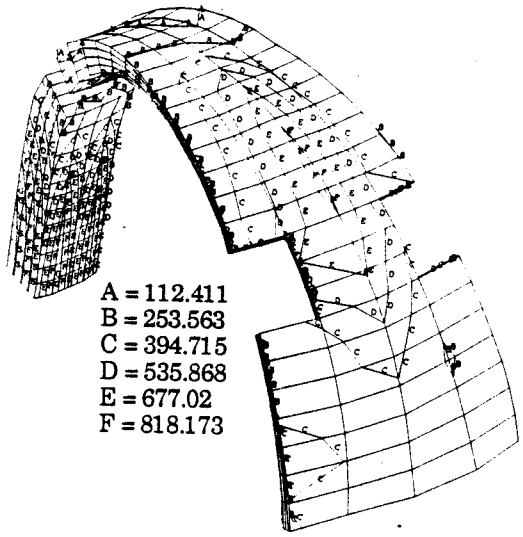

Figure 6a. Equivalent von-Mises structure in the bucking cylinder and structure with structural caps.

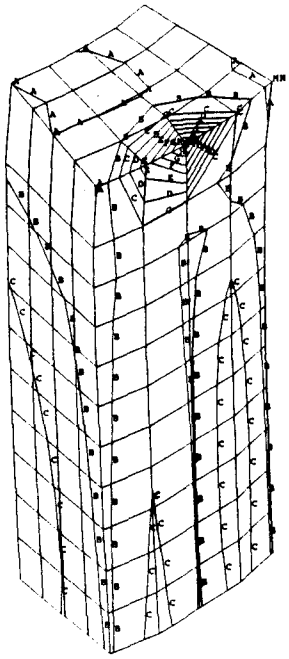

Figure 6b. Equivalent von-Mises structure in the bucking cylinder and structure without structural caps.

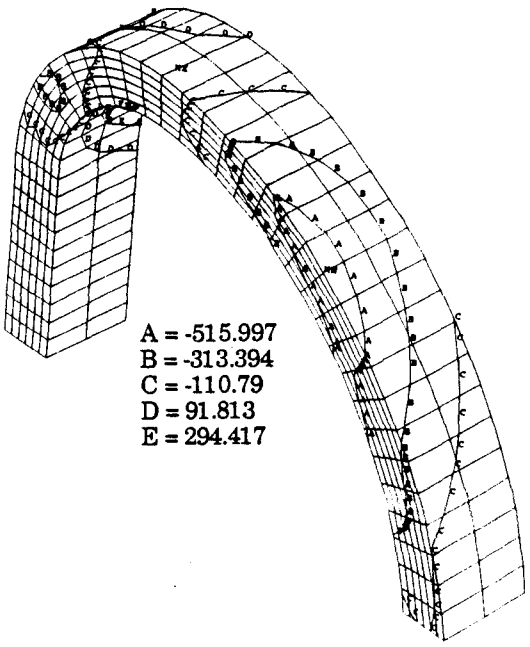

Figure 7b. Shear stresses τ_{xy} in the coil without structural caps.

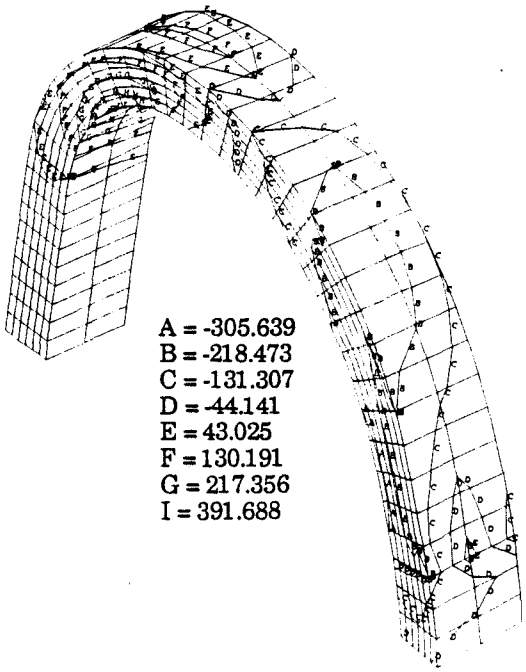

Figure 7a. Shear stresses τ_{xy} in the coil with structural caps.

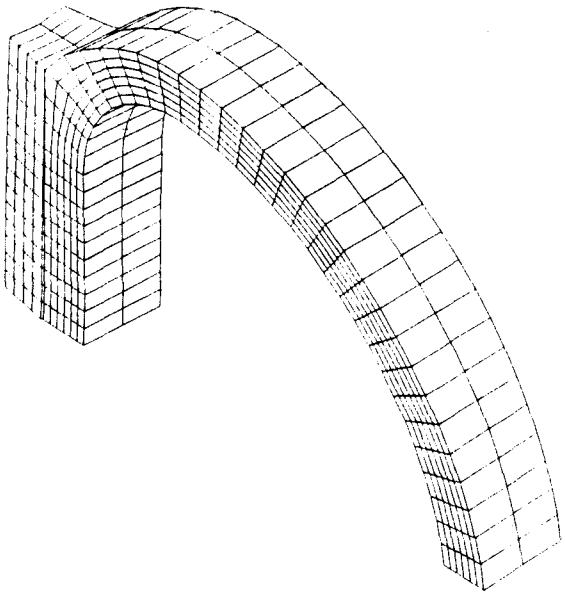

Figure 8. FEM Model with higher bucking cylinder.

5. Summary

A novel scheme for improving the structural, electrical, and cryogenic behaviour of the plate magnets has been studied. It offers increased flexibility as compared to other winding methods. Structurally, the coils behave as a monolith. If coupled to a bucking cylinder and modest structural caps, the coils are able to support the normal out-of-plane coils without the need for a large intercoil structure, increasing the access and maintainability of the reactor.

The caps reduce the stresses in the outer regions of the coils by about 300 MPa in normal operation. It also is needed for off-normal load conditions. Further work needs to be done in order to fully understand the tradeoffs between the different methods of winding. In particular, it is necessary to analyze the details of the conductor-shell interface. The conductors serve as keys between shells by transmitting shear. The effect of the shear on the superconductor needs to be assessed. Off-normal loads (disruptions, coil failures) in the magnet system also need to be investigated. Detailed modeling of the shell-to-shell interface inside each toroidal field coil remains to be done.

The novel configuration may offer advantages for manufacturing, structural behaviour (monolithic), and access and maintainability (due to the minimization of out-of-plane structure).

This work was supported by the U. S. Department of Energy Contract No. DE-FG02-91ER-54110.

References

[1] "IAEA Large Coil Task; Chapter 3: Characteristics of the Coils," D. S. Beard, W. Klose, S. Shimamoto, and G. Vecsey, eds., Fusion Eng. & Des. **7** 23 (1988).

[2] H. Schultz, F. S. Malick, D. R. Cohn, and J. E. C. Williams, "High Field Compact Tokamak Reactor," in Proc. 8th Symp.of Fusion Research (1979).

[3] L. Bromberg, D. R. Cohn, J. Schultz, J. Schwartz, P. Titus, J. E. C. Williams, S. P. Grotz, R. L. Creedon, and C. P. C. Wong,"Magnet Design for the ARIES-I High Field Tokamak Reactor," Fusion Tech. 1990, BV.E. Keen, M. Huguet, R. Hemsworth, eds., Elsevier Science Publishers B.V. (1991).

[4] J. Schwartz, L. Bromberg, D. R. Cohn, and J. E. C. Williams, "A Commercial Tokamak Reactor Using Super High Field Superconducting Magnets," Fusion Tech. **15** 957 (1989).

[5] F. Najmabadi, R. W. Conn, and The ARIES Team, "The ARIES-I Tokamak Reactor Study - Final Report," UCLA Report, UCLA-PPG 1323 (1991).